

This Dissertation
entitled
ADSORBATE INDUCED RECONSTRUCTIONS OF METAL SURFACES
typeset with $\text{NDDiss2}_{\mathcal{E}}$ v3.2013 (2013/04/16) on December 31, 2015 for
Joseph R. Michalka

This L^AT_EX 2 _{\mathcal{E}} classfile conforms to the University of Notre Dame style guidelines as of Fall 2012. However it is still possible to generate a non-conformant document if the instructions in the class file documentation are not followed!

Be sure to refer to the published Graduate School guidelines at <http://graduateschool.nd.edu> as well. Those guidelines override everything mentioned about formatting in the documentation for this NDDiss2 _{\mathcal{E}} class file.

It is YOUR responsibility to ensure that the Chapter titles and Table caption titles are put in CAPS LETTERS. This classfile does *NOT* do that!

*This page can be disabled by specifying the “noinfo” option to the class invocation.
(i.e., \documentclass[... , noinfo]{nddiss2e})*

This page is *NOT* part of the dissertation/thesis. It should be disabled before making final, formal submission, but should be included in the version submitted for format check.

NDDiss2 _{\mathcal{E}} documentation can be found at these locations:

<http://www.gsu.nd.edu>
<http://graduateschool.nd.edu>

ADSORBATE INDUCED RECONSTRUCTIONS OF METAL SURFACES

A Dissertation

Submitted to the Graduate School
of the University of Notre Dame
in Partial Fulfillment of the Requirements
for the Degree of

Doctor of Philosophy

by
Joseph R. Michalka

J. Daniel Gezelter, Director

Graduate Program in Chemistry and Biochemistry

Notre Dame, Indiana

December 2015

ADSORBATE INDUCED RECONSTRUCTIONS OF METAL SURFACES

Abstract

by

Joseph R. Michalka

In this dissertation I present work on the modeling of adsorbate-metal interactions with a specific focus on Carbon Monoxide (CO) induced restructuring of Platinum stepped surfaces. Additionally, I will present work on the development of a multiple-minima fluctuating charge (MM-flucQ) potential which has been used to simulate charge transfer and oxide formation on Platinum surfaces.

New Pt-CO and Au-CO forcefields were developed to study coverage-dependent restructuring of high-index Platinum & Gold (557) surfaces. It was observed that the weak Au-CO binding led to minimal disruption of the surface, whereas the strong Pt-CO interactions resulted in significant disruption of the step-edges which led to increased step-wandering. Specifically, the strong CO-CO quadrupolar repulsion caused an increase in adatom mobility. This increased mobility eventually led to large-scale surface reconstructions.

A Platinum/Palladium (557) surface was simulated to explore the interplay between CO-induced reconstruction on a more complicated bimetallic surface. The Pt-CO forcefield was retuned while a new Pd-CO forcefield was developed. The difference in binding strengths was found to play an important role in the disruption of the Pt/Pd surface while the preferred binding sites on each system (Pt: atop, Pd: bridge/hollow) led to different behaviors with regards to surface diffusion and mobility.

The importance of step-edges energetics for the formation of adatoms as observed from earlier work encouraged us to directly examine the differences between straight edged (557) & (112) and kinked edged (765) & (321) Pt surfaces. As hypothesized, the systems with rougher edges experienced a greater amount of surface diffusion and a concomitantly increased amount of step-wandering. The length of the (111) plateaus between step edges also played an important role with regard to the extent of surface reconstruction observed.

Accurate treatment of the electrostatic interactions between adsorbates and surfaces is often neglected in molecular dynamics simulations because of the increased computational cost and difficulty of implementation. Our new MM-flucq potential allows us to more properly describe a metal surface's response to impinging charged species in a dynamic fashion by allowing the charges on each atomic site to fluctuate in response to the local electronic environment.

DEDICATION

To my wife and family, and the many great teachers who have always believed in
me.

CONTENTS

| | |
|--|------|
| FIGURES | v |
| TABLES | viii |
| ACKNOWLEDGMENTS | ix |
| CHAPTER 1: INTRODUCTION | 1 |
| 1.1 Metals | 2 |
| 1.1.1 Structure | 2 |
| 1.1.1.1 Bimetallic Systems | 4 |
| 1.1.2 Dynamics | 4 |
| 1.1.2.1 Diffusion & Step-Wandering | 4 |
| 1.2 Adsorbate Interactions on Metal Surfaces | 6 |
| 1.2.1 Binding Sites | 6 |
| 1.2.2 Coverage Dependence | 6 |
| 1.2.2.1 Patterning | 8 |
| 1.3 Adsorbate Induced Reconstructions | 8 |
| 1.3.1 Refaceting | 8 |
| 1.3.1.1 Doubling | 9 |
| 1.3.2 Island Formation | 9 |
| CHAPTER 2: MOLECULAR DYNAMICS SIMULATIONS OF THE SURFACE RECONSTRUCTIONS OF PT(557) AND AU(557) UNDER EXPOSURE TO CO | 10 |
| 2.1 Introduction | 10 |
| 2.2 Simulation Methods | 11 |
| 2.2.1 Metal-metal interactions | 12 |
| 2.2.2 Carbon Monoxide model | 13 |
| 2.2.3 Cross-Interactions between the metals and carbon monoxide . . | 14 |
| 2.2.4 Force field validation | 17 |
| 2.2.5 Pt(557) and Au(557) metal interfaces | 20 |
| 2.3 Results | 21 |
| 2.3.1 Structural remodeling | 21 |
| 2.3.1.1 Step wandering | 21 |
| 2.3.1.2 Double layers | 22 |

| | | |
|---|---|----|
| 2.3.2 | Dynamics | 23 |
| 2.3.2.1 | Transport of surface metal atoms | 24 |
| 2.3.2.2 | Dynamics of double layer formation | 27 |
| 2.4 | Discussion | 28 |
| 2.4.1 | Diffusion | 28 |
| 2.4.2 | Mechanism for restructuring | 28 |
| 2.4.3 | CO Removal and double layer stability | 35 |
| 2.5 | Conclusion | 36 |
| CHAPTER 3: CO-INDUCED ISLAND FORMATION ON PT/PD(557) SURFACE ALLOYS: A MOLECULAR DYNAMICS STUDY | | 38 |
| 3.1 | Introduction | 38 |
| 3.2 | Methodology | 39 |
| 3.2.1 | Interaction Potentials | 39 |
| 3.2.2 | (557) Interfaces and surface alloys | 44 |
| 3.2.3 | Analysis of surface features and adatom diffusion | 46 |
| 3.3 | Results | 46 |
| 3.3.1 | Structural changes | 46 |
| 3.3.2 | Transport of surface metal atoms | 47 |
| 3.3.3 | Pt island formation on the Pt/Pd alloy | 48 |
| 3.4 | Discussion | 54 |
| 3.4.1 | Structural changes | 54 |
| 3.4.2 | Surface adatom formation | 55 |
| 3.5 | Summary | 58 |
| CHAPTER 4: EFFECTS OF STEP-TYPE ON THE CO-INDUCED SURFACE RECONSTRUCTIONS OF PT(557)/(112)/(321)/(765) FACETS | | 60 |
| CHAPTER 5: DEVELOPMENT OF A MULTIPLE-MINIMA FLUCTUATING CHARGE (MM-FLUCQ) POTENTIAL | | 61 |
| CHAPTER 6: SUMMARY | | 62 |
| BIBLIOGRAPHY | | 63 |

FIGURES

- 1.1 On the left are displayed face-down views of common low-index facets of metals (a) (100), (b) (110), and (c) (111). The dotted lines represent a repeatable crystal unit on each facet. The light gray coloring in (b) is illustrating the placement of that row of atoms beneath the top and bottom row. Facet (d) displays a (112) step edge. The darker shading represents separate terraces that are displaced by one atomic height.

1.2 The top two systems are $\text{Pd}_{0.5}\text{Pt}_{0.5}$ homogeneous alloys, with the left representing a flat plane and the right image depicting a 30 Ånanosphere. The bottom left image displays a near-surface alloy with one layer of Pd sandwiched between layers of Pt while the right image shows a core-shell nanosphere with a small section cut away to allow the thickness of the shell to be observed.

1.3 The atop (green), bridge (blue), and three-fold hollow (red) adsorption sites are the three most common binding sites for small molecules on low energy surfaces. Depending on the energy levels of the adsorbate orbitals that engage in bonding there will be varying preferences for binding sites. Carbon monoxide's 4444 orbital is well-matched with platinum's 4444 orbital leading to an atop preference, whereas on palladium, CO is more energetically stable in the bridge or hollow site. . .

2.1 The Pt(557) / 50% CO interface upon exposure to the CO: (a) 258 ps, (b) 19 ns, (c) 31.2 ns, and (d) 86.1 ns after exposure. Disruption of the (557) step-edges occurs quickly. The doubling of the layers appears only after two adjacent step-edges touch. The circled spot in (b) nucleated the growth of the double step observed in the later configurations.

2.2 Diffusion constants for mobile surface atoms along directions parallel ($\mathbf{D}_{||}$) and perpendicular (\mathbf{D}_{\perp}) to the (557) step-edges as a function of CO surface coverage. The two reported diffusion constants for the 50% Pt system correspond to a 20 ns period before the formation of the double layer (upper points), and to the full 40 ns sampling period (lower points).

| | |
|--|----|
| 2.3 Configurations used to investigate the mechanism of step-edge breakup on Pt(557). In each case, the central (starred) atom was pulled directly across the surface away from the step edge. The Pt atoms on the upper terrace are colored dark grey, while those on the lower terrace are in white. In each of these configurations, some of the atoms (highlighted in blue) had CO molecules bound in the vertical atop position. The energies of these configurations as a function of central atom displacement are displayed in Figure 2.4. | 31 |
| 2.4 Energies for displacing a single edge atom perpendicular to the step edge as a function of atomic displacement. Each of the energy curves corresponds to one of the labeled configurations in Figure 2.3, and the energies are referenced to the unperturbed step-edge. Certain arrangements of bound CO (notably configurations g and h) can lower the energetic barrier for creating an adatom relative to the bare surface (configuration a). | 32 |
| 2.5 Points along a possible reaction coordinate for CO-mediated edge doubling. Here, a CO-bound adatom burrows into an established step edge and displaces an edge atom onto the upper terrace along a curvilinear path. The approximate barrier for the process is 20 kcal/mol, and the complete process is exothermic by 15 kcal/mol in the presence of CO, but is endothermic by 3 kcal/mol without CO. | 34 |
| 2.6 Behavior of an established (111) double step after removal of the adsorbed CO: (A) 0 ps, (B) 100 ps, and (C) 1 ns after the removal of CO. Nearly immediately after the CO is removed, the step edge reforms in a (100) configuration, which is also the step type seen on clean (557) surfaces. The step separation involves significant mixing of the lower and upper atoms at the edge. | 36 |
| 3.1 Analysis of the surface alloy to find surface domain sizes was carried out by mapping the surface composition (left) onto 1 Å spaced grid points (center). Contiguous domains were identified and have been shown in distinct colors (right), and the distribution of domain areas was collected over 18 ns time windows. | 47 |
| 3.2 Snapshots of some of the simulated systems highlighting the (557) step edges (top) along with a diagonal view (bottom). System (a) is the pure Pd (557) ~40 ns after being dosed with 0.5 ML of CO. System (b) is the bare surface alloy after ~110 ns at 850 K, while (c) is the surface alloy ~110 ns after exposure to 0.5 ML of CO. Pt atoms are shown in gray, Pd in pink, while the adsorbed CO molecules are shown in silver / red. | 48 |
| 3.3 Distributions of Pd domain sizes at different CO coverages and at different times after exposure to CO. | 50 |
| 3.4 Distributions of Pt domain sizes at different CO coverages and at different times after exposure to CO. | 51 |

| | | |
|-----|--|----|
| 3.5 | Population of Pt atoms with either 6 (solid), 9 (dashed), or ≥ 10 (dot-dashed) Pt nearest neighbors averaged over 18 ns blocks of time. At $t = 0$, the majority (2/3) of Pt is located in the (111) plateaus where the number of Pt nearest neighbors is 6. The remaining Pt is located at step edges, with a nearest neighbor Pt count of 5. | 52 |
| 3.6 | The relative energies for moving a Pd atom (marked with an asterisk) perpendicular to a (557) step edge. This atom is translated across the bare Pd surface in curve A. The presence of one or two CO molecules bound in bridge sites near the edge significantly stabilizes the edge atom (curves B and C). If CO is bound to the edge atom in either a bridge (curves D and E) or hollow (curve F) site, the barrier is increased. | 56 |
| 3.7 | The relative energies for moving a step-edge Pt atom (marked with an asterisk) perpendicular to a (557) step edge. As in figure 3.6, the bare surface is shown in curve A. The presence of atop-bound CO molecules on the edge atom and at nearby sites can lower the energy for adatom formation (e.g. curves E, G, and H). | 57 |

TABLES

| | | |
|-----|---|----|
| 2.1 | POSITIONS, LENNARD-JONES PARAMETERS (σ AND ϵ), AND CHARGES FOR CO-CO INTERACTIONS | 14 |
| 2.2 | PARAMETERS FOR THE METAL-CO CROSS-INTERACTIONS | 16 |
| 2.3 | ADSORPTION ENERGIES FOR CO ON M(111) | 16 |
| 2.4 | RELATIVE ENERGIES OF (S)INGLE M(557) AND (D)OUBLE-STEP RECONSTRUCTIONS | 19 |
| 3.1 | PARAMETERS FOR THE METAL-CO CROSS-INTERACTIONS | 42 |
| 3.2 | ADSORPTION ENERGIES FOR A CO MOLECULE AT THE THREE PRIMARY BINDING SITES ON M(111) | 43 |
| 3.3 | FRACTION OF MOBILE PT SURFACE ATOMS AND THEIR SURFACE DIFFUSION | 49 |
| 3.4 | CHANGE IN PD SURFACE COVERAGE OVER SIMULATION | 53 |

ACKNOWLEDGMENTS

My time at graduate school has been a long road that has been greatly enriched by my many fantastic colleagues and mentors. I would like to especially thank my advisor, Professor J. Daniel Gezelter, for his guidance and support throughout this research. His piercing insights, expertise in coding, and skills as a teacher have helped me grow as a researcher and a teacher. I am indebted to my former and present group members and colleagues, Dr. Shenyu Kuang, Dr. James Marr, Dr. Kelsey Stocker, Dr. Zack Terranova, Dr. Mary Sherman, Madan Lamichhane, Patrick Louden, Suzanne Neidhart, Patrick McIntyre, Heather Chiarello, Andrew Latham, and Thomas Parsons for many helpful discussions, research related or otherwise.

I am extremely grateful to the Kaneb Center and its staff, especially Kristi Rudenga, as well as my co-graduate student associates, Andre Audette, Amy Buchmann, Justus Ghormley, Megan Hall, and Kelly Warmuth (Kuznicki) for many great discussions and workshops filled with teaching and pedagogy. I also owe many thanks to Dr. Lappin, James Johnson, Sarah West, Steven Weitstock, and Dr. Gezelter for the experience I gained while assisting them in classes and labs.

I am very thankful to my committee members, Professor J. Daniel Gezelter, Professor Steven A. Corcelli, and Professor Gregory V. Hartland for their many helpful questions and challenges to help me navigate through this process.

I must not forgot to mention the administrative assistance and encouragement I received from Deb Bennet, Cheryl Copley, Amanda Huerta, and the rest of the Chemistry and Biochemistry Department.

Finally, I would like to acknowledge my best friend and wife, Karen Hooge

Michalka. The love and support she has shown me throughout my time at Notre Dame, especially while I have been writing and applying for jobs has helped more than she knows.

CHAPTER 1

INTRODUCTION

Metal surfaces and nanoparticles play a role in many areas of chemistry, including catalysis[], energy generation[], and biomedical applications.[82] The differences in their displayed facets and morphologies can play a significant role in their activity[], selectivity[], and stability[132, 130]. Bimetallic species and alloys[], along with supported surfaces and supported nanoparticles[] allow for an even greater design space for various mechanical[13, 48], optical[], and catalytic properties[44] because of the modification of the electronic environment. In most practical applications the surface of the metal will be exposed to a variety of atmospheric compositions leading to various adsorbed species on the surface. For certain metals and conditions there is also the possibility of oxide formation which can dramatically change the surface properties for the material.[22] The interactions between metals and adsorbates adds an additional layer of complexity when attempting to fully describe metal surfaces because the presence of adsorbates will directly perturb the electronic environment and can even lead to reconstruction events that change the surface.[114, 112, 55] This dissertation is intended to provide a fundamental picture for adsorbate induced reconstruction on metal surfaces by examining the complex interactions present in these systems, measuring the perturbed dynamics, and analyzing the effect of different exposed facets by using Molecular Dynamics (MD) simulations to capture the atomic mechanisms that lead to restructuring.

This organization of this dissertation is such that a brief overview of metallic systems, adsorbate interactions, and adsorbate-induced reconstructions is presented

in Chapter 1. The second chapter presents work on the surface reconstructions of Pt (557) and Au (557) surfaces when exposed to carbon monoxide (CO). In Chapter 3 the effect of CO adsorption on a Pt/Pd (557) subsurface alloy is explored. The fourth chapter more fully examines the effects of step type and plateau length as they affect the CO-induced restructuring of platinum. Moving away from Pt-CO systems, Chapter 5 presents our development of the MM-flucQ potential and its applications to charge transfer and oxide formation on Pt surfaces. Finally, Chapter 6 contains a summary of this work as well as proposals for future directions.

1.1 Metals

The electronic properties of metals, as compared to other molecular species makes them particularly useful for a variety of chemical and material processes where their heterogenous bonding characteristics can be used effectively. The ease of movement of the valence electrons coupled with the band structure of the metallic orbitals gives metals many technologically useful characteristics including high electrical and thermal conductivity, malleability, and various optical properties that make them amenable for sensing applications and energy harvesting. With regards to catalytic activity, the metals in columns 9, 10, and 11 (Pt, Pd, Rh, etc.) of the periodic table tend to be highly active for catalytic processes because these metals typically have a larger valence electron density and the energy of the valence orbitals for these metals often matches up well with adsorbate orbitals leading to strong metal-adsorbate molecular interactions which often weakens the bonds within the adsorbate making scission more favorable.

1.1.1 Structure

The strength and type of allowed adsorbate bonding will be strongly dependent on the displayed surface structure of the metal. Most metals adopt either a face-centered

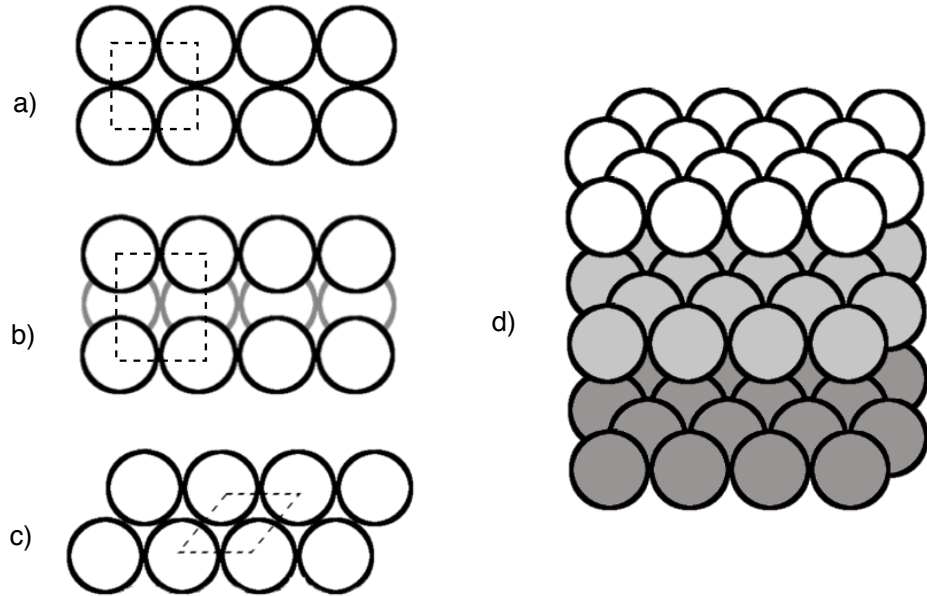


Figure 1.1. On the left are displayed face-down views of common low-index facets of metals (a) (100), (b) (110), and (c) (111). The dotted lines represent a repeatable crystal unit on each facet. The light gray coloring in (b) is illustrating the placement of that row of atoms beneath the top and bottom row. Facet (d) displays a (112) step edge. The darker shading represents separate terraces that are displaced by one atomic height.

cubic (FCC) or hexagonal close-packed (HCP) bulk crystal structure because this allows for the highest packing density. A more complicated surface can be prepared by cutting a bulk sample along nearly various sets of Miller indices. The different displayed facets have different surface energies and stabilities. The three common low energy facets are shown in Figure 1.1. For many metal surfaces, platinum and palladium specifically, the surface energy of the (111) facet is the most stable and barring kinetic barriers a higher-index, *i.e.* rougher, surface will minimize to this structure. The displayed low-energy structures are very important when considering how the metal will interact with adsorbates because the strength of the adsorption often depends on the displayed surface.

1.1.1.1 Bimetallic Systems

Since the properties and structure of metal systems are directly tied to their electronic nature, anything that perturbs the density of states will likely lead to deviations from bulk behavior. The presence of adsorbates or an electron-donating or withdrawing support, i.e. Al_2O_3 will perturb the system but one of the most powerful ways to design catalysts is through combining two or more metals together. Significant research has been directed at examining various bimetallic systems, including heterogenous and homogeneous alloys, core-shell nanoparticles, and near surface alloys. Figure 1.2 shows a number of examples. Since the proportion of each metal along with its arrangement can in theory be tailored, bimetallic systems allow for a high degree of tuning of various properties.

1.1.2 Dynamics

Low-index facets of metals at room temperature will not undergo much movement because they are already low on the potential energy surface. However, these systems are also rarely used in real-world applications. High-index surfaces and roughened nanoparticles have a larger number of low-coordinated surface atoms that also tend to be more active for catalytic processes. The local environment that enables them to bond strongly with adsorbates also can lead to easier adatom formation and surface mobility. Repeated patterning, as seen in step surfaces where a low-index plateau extends for some length and then another layer of the metal is laid on top, like a staircase, can prove especially useful because of the relatively easy characterization of the surface.

1.1.2.1 Diffusion & Step-Wandering

The two main types of movement that will occur on metals both involve adatoms. Independent adatom movement is the type most likely to be seen as one particle is

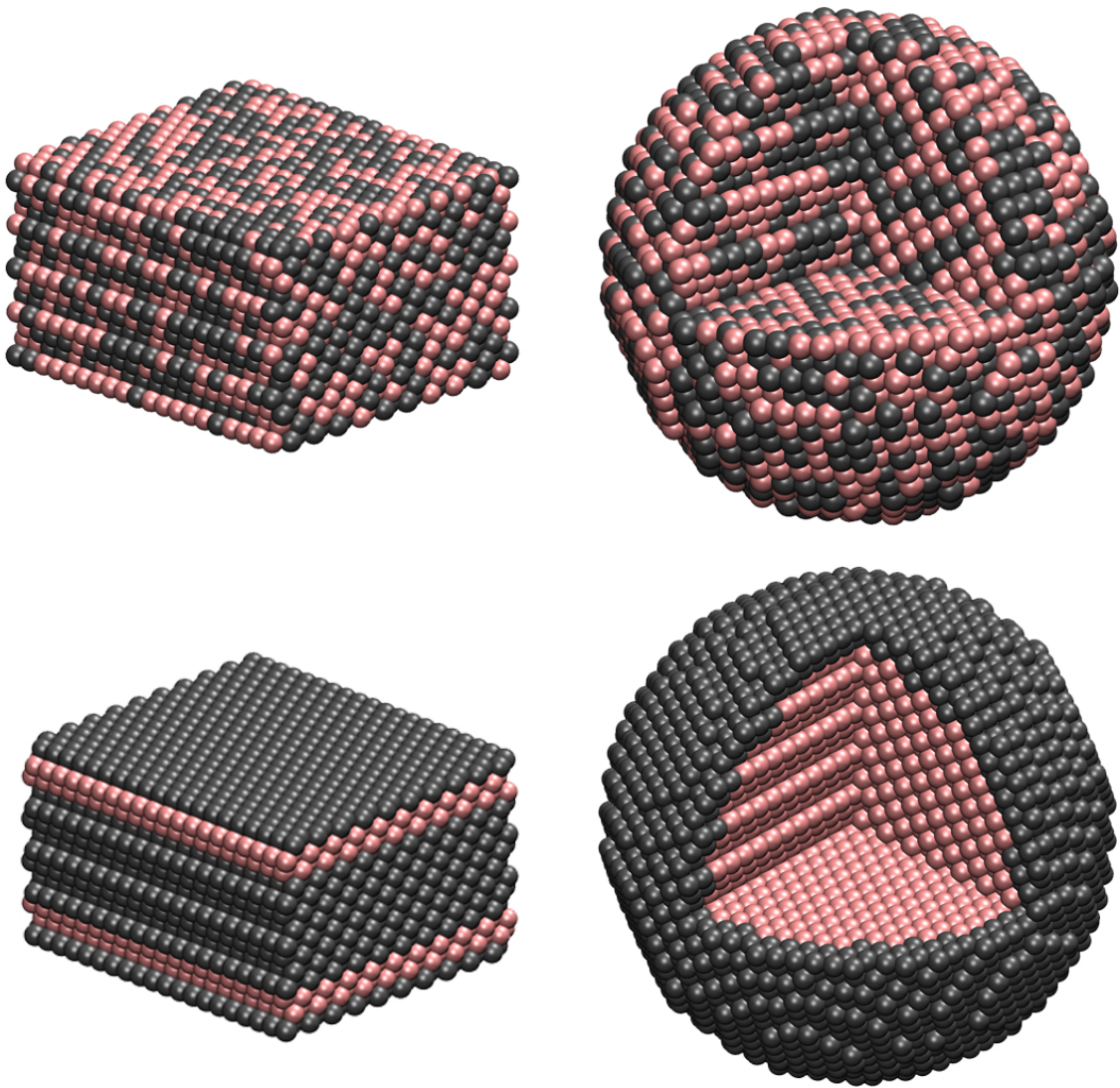


Figure 1.2. The top two systems are Pd_{0.5}Pt_{0.5} homogeneous alloys, with the left representing a flat plane and the right image depicting a 30 Ånanosphere. The bottom left image displays a near-surface alloy with one layer of Pd sandwiched between layers of Pt while the right image shows a coarse-shell nanosphere with a small section cut away to allow the thickness of the shell to be observed.

ejected from a stable edge or terrace and then explores the plateau around it. Since the strength of metallic bonding is tied to the number of nearest neighbors, once an adatom is created and is seated on the surface, there is often only a minimal energy barrier for it to continue exploring the surface.

The second main type of movement involves cooperative adatom diffusion and is better described as entire step-edges “wandering” on the surface. This wandering is ultimately a collection of ejection and readsorption events of surface metal atoms but it is more helpful to look at the collective motion than all of the individual motions.

1.2 Adsorbate Interactions on Metal Surfaces

The majority of applications involving metals ultimately involve the metal surface providing a favorable environment for some other reaction to occur, whether that be oxidation of CO, production of H₂ through a water-gas-shift reaction, or some other mechanism that involves molecules adsorbing to a surface. Having an accurate understanding of how adsorbates interact with metal surfaces is thus of the utmost importance.

1.2.1 Binding Sites

Generally, a surface with a lower index has less electron density to contribute to a potential adsorbate, weakening the strength of the binding. However, the orbitals of the adsorbate also play a role in binding preference. The three most common binding sites on a (111) facet are highlighted in Figure 1.3.

1.2.2 Coverage Dependence

While there might be one preferred binding site for a single adsorbate on a metal surface, the presence of strong adsorbate-adsorbate interactions can lead to deviations from expected behavior. While adsorbate-adsorbate interaction are often repulsive or

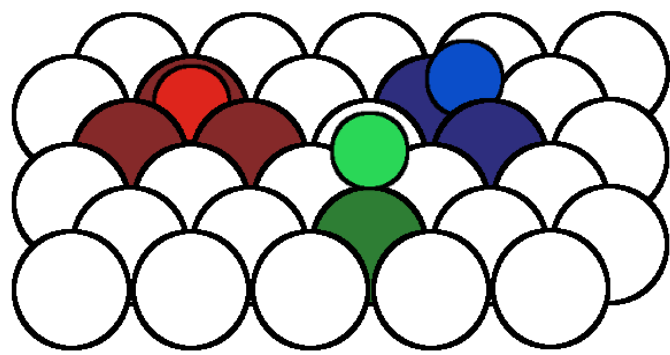


Figure 1.3. The atop (green), bridge (blue), and three-fold hollow (red) adsorption sites are the three most common binding sites for small molecules on low energy surfaces. Depending on the energy levels of the adsorbate orbitals that engage in bonding there will be varying preferences for binding sites. Carbon monoxide's 4444 orbital is well-matched with platinum's 4444 orbital leading to an atop preference, whereas on palladium, CO is more energetically stable in the bridge or hollow site.

induce strain in the metal surface making the binding weaker[25] it has been shown that cooperative effects can also arise when adsorbates are absorbed in different electronic environments. It has been predicted that while CO prefers the atop site on Pt at low coverages, as the coverage approaches 0.5 monolayers the binding preference changes to a mixed atop/bridge (CHECK) configuration because of favorable dipole-dipole interactions that result due to non-equivalent charge transfer from the Pt back into the CO orbitals. Since the presence and configuration of adsorbates

1.2.2.1 Patterning

1.3 Adsorbate Induced Reconstructions

While metal surfaces often remain stable even when the environment is perturbed, some situations can arise where the presence of adsorbates sufficiently modify the potential energy surface so that a new facet is energetically preferred. This situation might even be commonplace, but altering the potential energy surface only solves part of the problem. The system must also be able to overcome any kinetic barriers that would prevent the restructuring from taking place. For systems that are started in a high-index configuration, e.g. nanocubes and nanospheres, that are only in these configurations because of kinetic barriers, the introduction of adsorbates will likely lead to a restructuring to a lower-energy structure.

The time and length scales of these reconstruction processes vary widely[] and while current experimental techniques are able to observe and identify the reconstructions, they are often unable to identify the mechanisms of restructuring, which are important for designing catalysts.

1.3.1 Refaceting

Surfaces will refacet if they were originally cut at too high of an angle. This has been explored previously for a number of systems[51] and the refaceting will continue

until REPLACE WITH EQUATION ABOUT STABILITY. This restructuring typically only occurs in the forward direction while the presence of adsorbates can induce this reconstruction, a temperature increase will also likely allow this to occur since it is most likely that there is just a kinetic barrier that must be overcome.

1.3.1.1 Doubling

Work by Tao *et al.* on a Pt (557) surface exposed to CO observed a reversible reconstruction event that was directly dependent on the presence of CO in the system. When CO was introduced the step-edges doubled, but upon removal of the CO the original (557) motif was recovered. This reversible reconstruction strongly implies that the presence of CO temporally modifies the potential energy surface to prefer a new ground state structure; however, the exact mechanism of this reconstruction was not deduced at the time. This dissertation originally started as an attempt to model this system and attempt to provide insights into the mechanism of reconstruction.

1.3.2 Island Formation

Since catalytic reactions typically only occur at the surface, significant research has been devoted to increasing the surface area to bulk ratio of metal catalysts, either through catalyst supports, high-index nanostructures, or bimetallic near surface alloys. While these systems are typically stable at low temperatures and pressures, significant perturbations can lead to what is effectively sintering or island-formation of one of the metals on the surface. The interplay of surface energies and adsorbate interactions on two or more metal surfaces can lead to surprising results.

CHAPTER 2

MOLECULAR DYNAMICS SIMULATIONS OF THE SURFACE RECONSTRUCTIONS OF PT(557) AND AU(557) UNDER EXPOSURE TO CO

2.1 Introduction

Industrial catalysts usually consist of small particles that exhibit a high concentration of steps, kink sites, and vacancies at the edges of the facets. These sites are thought to be the locations of catalytic activity.[50, 63] There is now significant evidence that solid surfaces are often structurally, compositionally, and chemically modified by reactants under operating conditions.[111, 113, 110] The coupling between surface oxidation states and catalytic activity for CO oxidation on Pt, for instance, is widely documented.[28, 45] Despite the well-documented role of these effects on reactivity, the ability to capture or predict them in atomistic models is somewhat limited. While these effects are perhaps unsurprising on the highly disperse, multi-faceted nanoscale particles that characterize industrial catalysts, they are manifest even on ordered, well-defined surfaces. The Pt(557) surface, for example, exhibits substantial and reversible restructuring under exposure to moderate pressures of carbon monoxide.[113]

This work is an investigation into the mechanism and timescale for the Pt(557) & Au(557) surface restructuring using molecular simulation. Since the dynamics of the process are of particular interest, we employ classical force fields that represent a compromise between chemical accuracy and the computational efficiency necessary to simulate the process of interest. Since restructuring typically occurs as a result of

specific interactions of the catalyst with adsorbates, in this work, two metal systems exposed to carbon monoxide were examined. The Pt(557) surface has already been shown to undergo a large scale reconstruction under certain conditions.[113] The Au(557) surface, because of weaker interactions with CO, is less likely to undergo this kind of reconstruction. However, Peters *et al.*[85] and Piccolo *et al.*[86] have both observed CO-induced modification of reconstructions to the Au(111) surface. Peters *et al.* observed the Au(111)-(22 \times $\sqrt{3}$) “herringbone” reconstruction relaxing slightly under CO adsorption. They argued that only a few Au atoms become adatoms, limiting the stress of this reconstruction, while allowing the rest to relax and approach the ideal (111) configuration. Piccolo *et al.* on the other hand, saw a more significant disruption of the Au(111)-(22 \times $\sqrt{3}$) herringbone pattern as CO adsorbed on the surface. Both groups suggested that the preference CO shows for low-coordinated Au atoms was the primary driving force for the relaxation. Although the Au(111) reconstruction was not the primary goal of our work, the classical models we have fit may be of future use in simulating this reconstruction.

2.2 Simulation Methods

The challenge in modeling any solid/gas interface is the development of a sufficiently general yet computationally tractable model of the chemical interactions between the surface atoms and adsorbates. Since the interfaces involved are quite large (10^3 - 10^4 atoms), have many electrons, and respond slowly to perturbations, *ab initio* molecular dynamics (AIMD),[59, 58, 60] Car-Parrinello methods,[14, 49, 42] and quantum mechanical potential energy surfaces remain out of reach. Additionally, the “bonds” between metal atoms at a surface are typically not well represented in terms of classical pairwise interactions in the same way that bonds in a molecular material are, nor are they captured by simple non-directional interactions like the Coulomb potential. For this work, we have used classical molecular dynamics

with potential energy surfaces that are specifically tuned for transition metals. In particular, we used the EAM potential for Au-Au and Pt-Pt interactions.[36] The CO was modeled using a rigid three-site model developed by Straub and Karplus for studying photodissociation of CO from myoglobin.[106] The Au-CO and Pt-CO cross interactions were parameterized as part of this work.

2.2.1 Metal-metal interactions

Many of the potentials used for modeling transition metals are based on a non-pairwise additive functional of the local electron density. The embedded atom method (EAM) is perhaps the best known of these methods,[20, 36, 52, 19, 87, 119, 68, 2] but other models like the Finnis-Sinclair[34, 108] and the quantum-corrected Sutton-Chen method[56, 88] have simpler parameter sets. The glue model of Ercolessi *et al.*[27] is among the fastest of these density functional approaches. In all of these models, atoms are treated as a positively charged core with a radially-decaying valence electron distribution. To calculate the energy for embedding the core at a particular location, the electron density due to the valence electrons at all of the other atomic sites is computed at atom i 's location,

$$\bar{\rho}_i = \sum_{j \neq i} \rho_j(r_{ij})$$

Here, $\rho_j(r_{ij})$ is the function that describes the distance dependence of the valence electron distribution of atom j . The contribution to the potential that comes from placing atom i at that location is then

$$V_i = F[\bar{\rho}_i] + \sum_{j \neq i} \phi_{ij}(r_{ij})$$

where $F[\bar{\rho}_i]$ is an energy embedding functional, and $\phi_{ij}(r_{ij})$ is a pairwise term that is meant to represent the repulsive overlap of the two positively charged cores.

The EAM, Finnis-Sinclair, and the Quantum Sutton-Chen (QSC) potentials have all been widely used by the materials simulation community for simulations of bulk and nanoparticle properties,[17, 121, 72, 75] melting,[6, 97, 94] fracture,[100, 101, 76] crack propagation,[5, 91] and alloying dynamics.[102, 77, 133, 78] One of EAM’s strengths is its sensitivity to small changes in structure. This is due to the inclusion of up to the third nearest neighbor interactions during fitting of the parameters.[119] In comparison, the glue model of Ercolessi *et al.*[27] was only parameterized to include nearest-neighbor interactions, EAM is a suitable choice for systems where the bulk properties are of secondary importance to low-index surface structures. Additionally, the similarity of EAM’s functional treatment of the embedding energy to standard density functional theory (DFT) makes fitting DFT-derived cross potentials with adsorbates somewhat easier.

2.2.2 Carbon Monoxide model

Previous explanations for the surface rearrangements center on the large linear quadrupole moment of carbon monoxide.[113] We used a model first proposed by Karplus and Straub to study the photodissociation of CO from myoglobin because it reproduces the quadrupole moment well.[106] The Straub and Karplus model treats CO as a rigid three site molecule with a massless charge-carrying “M” site at the center of mass. The geometry and interaction parameters are reproduced in Table 2.1. The effective dipole moment, calculated from the assigned charges, is still small (0.35 D) while the linear quadrupole (-2.40 D Å) is close to the experimental (-2.63 D Å)[16] and quantum mechanical predictions (-2.46 D Å)[92].

TABLE 2.1
 POSITIONS, LENNARD-JONES PARAMETERS (σ AND ϵ), AND
 CHARGES FOR CO-CO INTERACTIONS

| | z^a | σ^a | ϵ^b | q^c |
|----------|---------|------------|--------------|-------|
| C | -0.6457 | 3.83 | 0.0262 | -0.75 |
| O | 0.4843 | 3.12 | 0.1591 | -0.85 |
| M | 0.0 | - | - | 1.6 |

The CO model from Ref. 106 was used without modification.

^a Distances are in Å.

^b Energies are in kcal/mol.

^c Charges are in a.u.

2.2.3 Cross-Interactions between the metals and carbon monoxide

Since the adsorption of CO onto a Pt surface has been the focus of much experimental 126, 47, 30, 53 and theoretical work 118, 57, 23, 31, 70 there is a significant amount of data on adsorption energies for CO on clean metal surfaces. An earlier model by Korzeniewski *et al.* 57 served as a starting point for our fits. The parameters were modified to ensure that the Pt-CO interaction favored the atop binding position on Pt(111). These parameters are reproduced in Table 2.2. The modified parameters yield binding energies that are slightly higher than the experimentally-reported values as shown in Table 2.3. Following Korzeniewski *et al.*, 57 the Pt-C interaction was fit to a deep Lennard-Jones interaction to mimic strong, but short-ranged, partial binding between the Pt *d* orbitals and the π^* orbital on CO. The Pt-O interaction was modeled with a Morse potential with a large equilibrium distance, (r_o). These choices ensure that the C is preferred over O as the surface-binding atom. In most

geometries, the Pt-O parameterization contributes a weak repulsion which favors the atop site. The resulting potential-energy surface suitably recovers the calculated Pt-C separation length (1.6 Å)¹¹⁸ and affinity for the atop binding position.^{24, 47}

The Au-C and Au-O cross-interactions were also fit using Lennard-Jones and Morse potentials, respectively, to reproduce Au-CO binding energies. The limited experimental data for CO adsorption on Au required refining the fits against plane-wave DFT calculations. Adsorption energies were obtained from gas-surface DFT calculations with a periodic supercell plane-wave basis approach, as implemented in the Quantum ESPRESSO package.⁴⁰ Electron cores were described with the projector augmented-wave (PAW) method,^{9, 61} with plane waves included to an energy cutoff of 20 Ry. Electronic energies are computed with the PBE implementation of the generalized gradient approximation (GGA) for gold, carbon, and oxygen that was constructed by Rappe, Rabe, Kaxiras, and Joannopoulos.^{84, 89} In testing the Au-CO interaction, Au(111) supercells were constructed of four layers of 4 Au x 2 Au surface planes and separated from vertical images by six layers of vacuum space. The surface atoms were all allowed to relax before CO was added to the system. Electronic relaxations were performed until the energy difference between subsequent steps was less than 10^{-8} Ry. Nonspin-polarized supercell calculations were performed with a 4 x 4 x 4 Monkhorst-Pack \mathbf{k} -point sampling of the first Brillouin zone.⁷⁹ The relaxed gold slab was then used in numerous single point calculations with CO at various heights (and angles relative to the surface) to allow fitting of the empirical force field.

The parameters employed for the metal-CO cross-interactions in this work are shown in Table 2.2 and the binding energies on the (111) surfaces are displayed in Table 2.3. Charge transfer and polarization are neglected in this model, although these effects could have an effect on binding energies and binding site preferences.

TABLE 2.2

PARAMETERS FOR THE METAL-CO CROSS-INTERACTIONS

| | σ^a | ϵ^b | | r^a | D^b | $\gamma (\text{\AA}^{-1})$ |
|-------------|------------|--------------|-------------|-------|-------|----------------------------|
| Pt-C | 1.3 | 15 | Pt-O | 3.8 | 3.0 | 1 |
| Au-C | 1.9 | 6.5 | Au-O | 3.8 | 0.37 | 0.9 |

Metal-C interactions are modeled with Lennard-Jones potentials, while the metal-O interactions were fit to broad Morse potentials.

^a Distances are given in Å

^b Energies are given in kcal/mol

TABLE 2.3

ADSORPTION ENERGIES FOR CO ON M(111)

| | Calculated ^a | Experimental ^a |
|--------------|-------------------------|---------------------------|
| Pt-CO | -1.81 | -1.4 (Ref. 53) |
| | | -1.9 (Ref. 126) |
| Au-CO | -0.39 | -0.40 (Ref. 26) |

The adsorption energies were calculated for a single CO molecule adsorbed vertically at an atop binding site on a (111) metal surface using the potentials described in this work

^a Adsorption energies are given in eV

2.2.4 Force field validation

The CO-Pt cross interactions were compared directly to DFT results found in the supporting information of reference 113. These energies are estimates of the degree of stabilization provided to double-layer reconstructions of the M(557) surface by an overlayer of CO molecules in a $c(2 \times 4)$ pattern. To make the comparison, five atom thick metal slabs of both Pt and Au displaying the (557) facet were constructed. Double-layer (reconstructed) systems were created using six atomic layers where enough of a layer was removed from both exposed (557) facets to create the double step. In all cases, the metal slabs contained 480 atoms and were minimized using steepest descent under the EAM force field. Both the bare metal slabs and slabs with 50% carbon monoxide coverage (arranged in the $c(2 \times 4)$ pattern) were used. The systems are periodic along and perpendicular to the step-edge axes with a large vacuum above the displayed (557) facet.

Energies computed using our force field are displayed in Table 2.4. The relative energies are calculated as $E_{relative} = E_{system} - E_{M(557)-S} - N_{CO} * E_{M-CO}(r)$, where $E_{M(557)-S}$ is the energy of a clean (557) surface. N_{CO} is the number of CO molecules present on the surface. In the $c(2 \times 4)$ patterning, the CO molecules relax to an average separation, r , from the nearest surface metal atom. $E_{M-CO}(r)$ is taken as the energy of a single CO molecule on a flat M(111) surface at a distance r from a metal atop site. These energies correspond to -1.8 eV for CO-Pt and -0.39 eV for CO-Au.

One important note is that the $c(2 \times 4)$ patterning on the stepped surfaces yields a slightly larger M-CO separation than one would find on a clean (111) surface. On a clean Pt(111) surface, for example, the optimized geometry has a C-Pt distance of 1.53 Å (corresponding to a binding energy of -1.83 eV). On the double-layer reconstruction and the single (557) step, the half monolayer optimizes to C-Pt separations of 1.58-1.60 Å, respectively. Although this difference seems quite small, there are

notable consequences for $E_{Pt-CO}(r)$ which then takes values from -1.815 eV to -1.8 eV.

For platinum, the bare double layer reconstruction is less stable than the bare (557) step by about 0.25 kcal/mol per Pt atom. However, addition of carbon monoxide changes the relative energetics of the two systems. This is a quite dramatic shift, $\Delta\Delta E$ (the change in energy for going from single to double-layer structures upon addition of a CO layer) shifts by -0.5 kcal/mol per Pt atom. This result is in qualitative agreement with the DFT calculations in reference 113, which also showed that the addition of CO leads to a reversal in stability.

The gold systems show a smaller energy difference between the clean single and double layers. Upon addition of CO, the single step surface is much more stable than the double-layer reconstruction. However, the CO-Au binding energy is much weaker, so at operating temperatures, the actual coverage by CO will be much lower than the 50% coverage afforded by the $c(2 \times 4)$ pattern, so single-point energy comparisons are not as helpful.

TABLE 2.4
RELATIVE ENERGIES OF (S)INGLE M(557) AND (D)OUBLE-STEP
RECONSTRUCTIONS

| Step | N_M | N_{CO} | Relative Energy | $\Delta E/N_M$ |
|-----------|-------|----------|-----------------|----------------|
| Pt(557)-S | 480 | 0 | 0 | 0 |
| Pt(557)-D | 480 | 0 | 119.788 | 0.2495 |
| Pt(557)-S | 480 | 40 | -109.734 | -0.2286 |
| Pt(557)-D | 480 | 48 | -110.039 | -0.2292 |
| Au(557)-S | 480 | 0 | 0 | 0 |
| Au(557)-D | 480 | 0 | 83.853 | 0.1747 |
| Au(557)-S | 480 | 40 | -253.604 | -0.5283 |
| Au(557)-D | 480 | 48 | -156.150 | -0.3253 |

The presence of a 50% coverage of CO in a $c(2 \times 4)$ pattern stabilizes the D-reconstructed Pt(557) surface, but leaves the S-unreconstructed Au(557) as the more stable structure

^a Energies are in kcal/mol

Qualitatively, our classical force field for the metal-CO cross interactions reproduces the results predicted by DFT studies in reference 113. Addition of polarization effects, both in the CO and in the metal surfaces, could make the model significantly more accurate. For example, because of the relatively large fixed charges, the current model will be unable to reproduce coverages in excess of 50% without forming an inverted CO second layer on the surface. The M-CO cross interactions would also be more accurate if they included the direct interactions between charges on the CO and their image charges inside the metal slab. These polarization effects have been

shown to play an important role,²⁴ and would be one way of improving the numerical agreement with quantum mechanical calculations.

2.2.5 Pt(557) and Au(557) metal interfaces

Our Pt system is an orthorhombic periodic box of dimensions $54.482 \times 50.046 \times 120.88 \text{ \AA}$ while our Au system has dimensions of $57.4 \times 51.9285 \times 100 \text{ \AA}$. The metal slabs are 9 and 8 atoms deep respectively, corresponding to a slab thickness of $\sim 21 \text{ \AA}$ for Pt and $\sim 19 \text{ \AA}$ for Au. The systems are arranged in a FCC crystal that have been cut along the (557) plane so that they are periodic in the x and y directions, and have been oriented to expose two aligned (557) cuts along the extended z -axis. Simulations of the bare metal interfaces at temperatures ranging from 300 K to 1200 K were performed to confirm the relative stability of the surfaces without a CO overlayer.

The different bulk melting temperatures predicted by EAM ($1345 \pm 10 \text{ K}$ for Au1 and $\sim 2045 \text{ K}$ for Pt7) suggest that any reconstructions should happen at different temperatures for the two metals. The bare Au and Pt surfaces were initially run in the canonical (NVT) ensemble at 800 K and 1000 K respectively for 100 ps. The two surfaces were relatively stable at these temperatures when no CO was present, but experienced increased surface mobility on addition of CO. Each surface was then dosed with different concentrations of CO that was initially placed in the vacuum region. Upon full adsorption, these concentrations correspond to 0%, 5%, 25%, 33%, and 50% surface coverage. Higher coverages resulted in the formation of a double layer of CO, which introduces artifacts that are not relevant to (557) reconstruction. Because of the difference in binding energies, nearly all of the CO was bound to the Pt surface, while the Au surfaces often had a significant CO population in the gas phase. These systems were allowed to reach thermal equilibrium (over 5 ns) before being run in the microcanonical (NVE) ensemble for data collection. All of the systems examined had at least 40 ns in the data collection stage, although simulation

times for some Pt of the systems exceeded 200 ns. Simulations were carried out using the open source molecular dynamics package, OpenMD.^{32, 73, 39}

2.3 Results

2.3.1 Structural remodeling

The bare metal surfaces experienced minor roughening of the step-edge because of the elevated temperatures, but the (557) face was stable throughout the simulations. The surfaces of both systems, upon dosage of CO, began to undergo extensive remodeling that was not observed in the bare systems. Reconstructions of the Au systems were limited to breakup of the step-edges and some step wandering. The lower coverage Pt systems experienced similar step edge wandering but to a greater extent. The 50% coverage Pt system was unique among our simulations in that it formed well-defined and stable double layers through step coalescence, similar to results reported by Tao *et al.*¹¹³

2.3.1.1 Step wandering

The bare surfaces for both metals showed minimal step-wandering at their respective temperatures. As the CO coverage increased however, the mobility of the surface atoms, described through adatom diffusion and step-edge wandering, also increased. Except for the 50% Pt system where step coalescence occurred, the step-edges in the other simulations preferred to keep nearly the same distance between steps as in the original (557) lattice, $\sim 13\text{\AA}$ for Pt and $\sim 14\text{\AA}$ for Au. Previous work by Williams *et al.*^{123, 122} highlights the repulsion that exists between step-edges even when no direct interactions are present in the system. This repulsion is caused by an entropic barrier that arises from the fact that steps cannot cross over one another. This entropic repulsion does not completely define the interactions between steps, however,

so it is possible to observe step coalescence on some surfaces.¹²³ The presence and concentration of adsorbates, as shown in this work, can affect step-step interactions, potentially leading to a new surface structure as the thermodynamic equilibrium.

2.3.1.2 Double layers

Tao *et al.*¹¹³ have shown experimentally that the Pt(557) surface undergoes two separate reconstructions upon CO adsorption. The first involves a doubling of the step height and plateau length. Similar behavior has been seen on a number of surfaces at varying conditions, including Ni(977) and Si(111).^{122, 123, 83} Of the two systems we examined, the Pt system showed a greater propensity for reconstruction because of the larger surface mobility and the greater extent of step wandering. The amount of reconstruction was strongly correlated to the amount of CO adsorbed upon the surface. This appears to be related to the effect that adsorbate coverage has on edge breakup and on the surface diffusion of metal adatoms. Only the 50% Pt surface underwent the doubling seen by Tao *et al.*¹¹³ within the time scales studied here. Over a longer time scale (150 ns) two more double layers formed on this surface. Although double layer formation did not occur in the other Pt systems, they exhibited more step-wandering and roughening compared to their Au counterparts. The 50% Pt system is highlighted in Figure 2.1 at various times along the simulation showing the evolution of a double layer step-edge.

The second reconstruction observed by Tao *et al.*¹¹³ involved the formation of triangular clusters that stretched across the plateau between two step-edges. Neither of the simulated metal interfaces, within the 40 ns time scale or the extended time of 150 ns for the 50% Pt system, experienced this reconstruction.

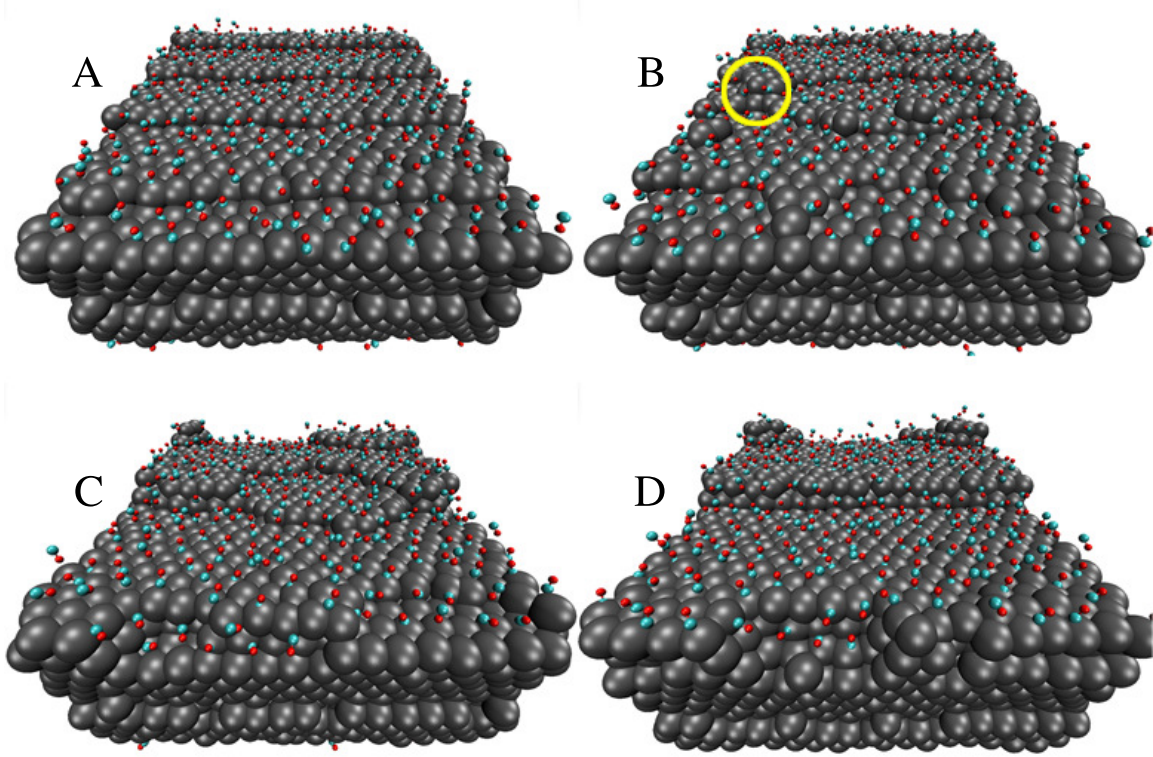


Figure 2.1. The Pt(557) / 50% CO interface upon exposure to the CO: (a) 258 ps, (b) 19 ns, (c) 31.2 ns, and (d) 86.1 ns after exposure. Disruption of the (557) step-edges occurs quickly. The doubling of the layers appears only after two adjacent step-edges touch. The circled spot in (b) nucleated the growth of the double step observed in the later configurations.

2.3.2 Dynamics

Previous experimental work by Pearl and Sibener⁸³, using STM, has been able to capture the coalescence of steps on Ni(977). The time scale of the image acquisition, ~ 70 s/image, provides an upper bound for the time required for the doubling to occur. By utilizing Molecular Dynamics we are able to probe the dynamics of these reconstructions at elevated temperatures and in this section we provide data on the timescales for transport properties, e.g. diffusion and layer formation time.

2.3.2.1 Transport of surface metal atoms

The wandering of a step-edge is a cooperative effect arising from the individual movements of the atoms making up the steps. An ideal metal surface displaying a low index facet, (111) or (100), is unlikely to experience much surface diffusion because of the large energetic barrier that must be overcome to lift an atom out of the surface. The presence of step-edges and other surface features on higher-index facets provides a lower energy source for mobile metal atoms. Using our potential model, single-atom break-away from a step-edge on a clean surface still imposes an energetic penalty around ~ 45 kcal/mol, but this is certainly easier than lifting the same metal atom vertically out of the surface, > 60 kcal/mol. The penalty lowers significantly when CO is present in sufficient quantities on the surface. For certain distributions of CO, the energetic penalty can fall to as low as ~ 20 kcal/mol. The configurations that create these lower barriers are detailed in the discussion section below.

Once an adatom exists on the surface, the barrier for diffusion is negligible (< 4 kcal/mol for a Pt adatom). These adatoms are then able to explore the terrace before rejoining either their original step-edge or becoming a part of a different edge. It is an energetically unfavorable process with a high barrier for an atom to traverse to a separate terrace although the presence of CO can lower the energy barrier required to lift or lower an adatom. By tracking the mobility of individual metal atoms on the Pt and Au surfaces we were able to determine the relative diffusion constants, as well as how varying coverages of CO affect the diffusion. Close observation of the mobile metal atoms showed that they were typically in equilibrium with the step-edges. At times, their motion was concerted, and two or more adatoms would be observed moving together across the surfaces.

A particle was considered “mobile” once it had traveled more than 2 \AA between saved configurations of the system (typically 10-100 ps). A mobile atom would typi-

cally travel much greater distances than this, but the 2 Å cutoff was used to prevent swamping the diffusion data with the in-place vibrational movement of buried atoms. Diffusion on a surface is strongly affected by local structures and the presence of single and double layer step-edges causes the diffusion parallel to the step-edges to be larger than the diffusion perpendicular to these edges. Parallel and perpendicular diffusion constants are shown in Figure 2.2. Diffusion parallel to the step-edge is higher than diffusion perpendicular to the edge because of the lower energy barrier associated with sliding along an edge compared to breaking away to form an isolated adatom.

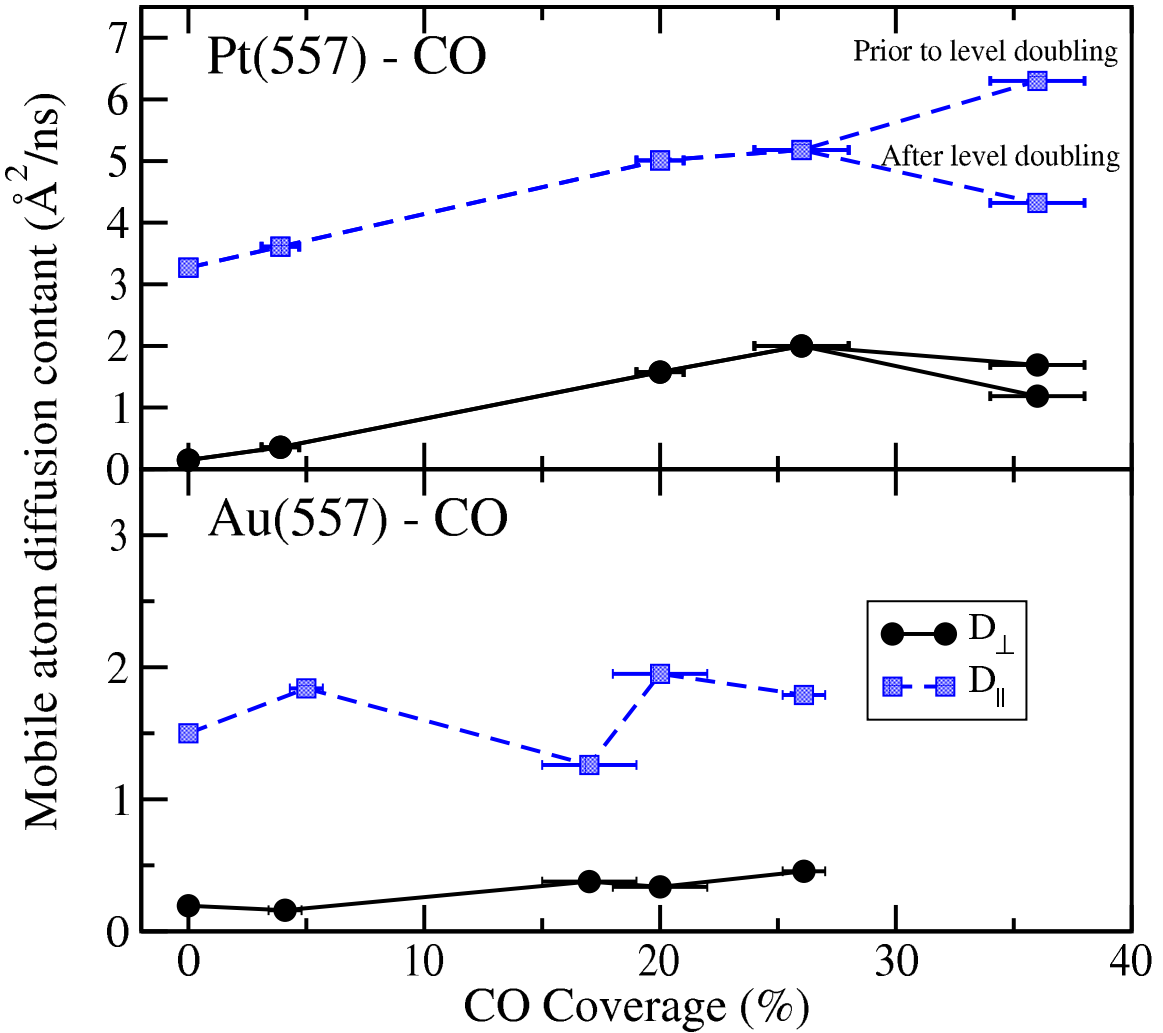


Figure 2.2. Diffusion constants for mobile surface atoms along directions parallel (D_{\parallel}) and perpendicular (D_{\perp}) to the (557) step-edges as a function of CO surface coverage. The two reported diffusion constants for the 50% Pt system correspond to a 20 ns period before the formation of the double layer (upper points), and to the full 40 ns sampling period (lower points).

The weaker Au-CO interaction is evident in the weak CO-coverage dependence of Au diffusion. This weak interaction leads to lower observed coverages when compared to dosage amounts. This further limits the effect the CO can have on surface

diffusion. The correlation between coverage and Pt diffusion rates shows a near linear relationship at the earliest times in the simulations. Following double layer formation, however, there is a precipitous drop in adatom diffusion. As the double layer forms, many atoms that had been tracked for mobility data have now been buried, resulting in a smaller reported diffusion constant. A secondary effect of higher coverages is CO-CO cross interactions that lower the effective mobility of the Pt adatoms that are bound to each CO. This effect would become evident only at higher coverages. A detailed account of Pt adatom energetics follows in the Discussion.

2.3.2.2 Dynamics of double layer formation

The increased diffusion on Pt at the higher CO coverages is the primary contributor to double layer formation. However, this is not a complete explanation – the 33% Pt system has higher diffusion constants, but did not show any signs of edge doubling in 40 ns. On the 50% Pt system, one double layer formed within the first 40 ns of simulation time, while two more were formed as the system was allowed to run for an additional 110 ns (150 ns total). This suggests that this reconstruction is a rapid process and that the previously mentioned upper bound is a very large overestimate.^{123, 83} In this system the first appearance of a double layer appears at 19 ns into the simulation. Within 12 ns of this nucleation event, nearly half of the step has formed the double layer and by 86 ns the complete layer has flattened out. From the appearance of the first nucleation event to the first observed double layer, the process took \sim 20 ns. Another \sim 40 ns was necessary for the layer to completely straighten. The other two layers in this simulation formed over periods of 22 ns and 42 ns respectively. A possible explanation for this rapid reconstruction is the elevated temperatures under which our systems were simulated. The process would almost certainly take longer at lower temperatures. Additionally, our measured times for completion of the doubling after the appearance of a nucleation site

are likely affected by our periodic boxes. A longer step-edge will likely take longer to “zipper”.

2.4 Discussion

We have shown that a classical potential is able to model the initial reconstruction of the Pt(557) surface upon CO adsorption, and have reproduced the double layer structure observed by Tao *et al.*¹¹³. Additionally, this reconstruction appears to be rapid – occurring within 100 ns of the initial exposure to CO. Here we discuss the features of the classical potential that are contributing to the stability and speed of the Pt(557) reconstruction.

2.4.1 Diffusion

The perpendicular diffusion constant appears to be the most important indicator of double layer formation. As highlighted in Figure 2.1, the formation of the double layer did not begin until a nucleation site appeared. Williams *et al.*^{123, 122} cite an effective edge-edge repulsion arising from the inability of edge crossing. This repulsion must be overcome to allow step coalescence. A larger \mathbf{D}_\perp value implies more step-wandering and a larger chance for the stochastic meeting of two edges to create a nucleation point. Diffusion parallel to the step-edge can help “zipper” up a nascent double layer. This helps explain the rapid time scale for double layer completion after the appearance of a nucleation site, while the initial appearance of the nucleation site was unpredictable.

2.4.2 Mechanism for restructuring

Since the Au surface showed no large scale restructuring in any of our simulations, our discussion will focus on the 50% Pt-CO system which did exhibit doubling.

A number of possible mechanisms exist to explain the role of adsorbed CO in restructuring the Pt surface. Quadrupolar repulsion between adjacent CO molecules adsorbed on the surface is one possibility. However, the quadrupole-quadrupole interaction is short-ranged and is attractive for some orientations. If the CO molecules are “locked” in a vertical orientation, through atop adsorption for example, this explanation would gain credence. Within the framework of our classical potential, the calculated energetic repulsion between two CO molecules located a distance of 2.77 Å apart (nearest-neighbor distance of Pt) and both in a vertical orientation, is 8.62 kcal/mol. Moving the CO to the second nearest-neighbor distance of 4.8 Å drops the repulsion to nearly 0. Allowing the CO to rotate away from a purely vertical orientation also lowers the repulsion. When the carbons are locked at a distance of 2.77 Å, a minimum of 6.2 kcal/mol is reached when the angle between the 2 CO is $\sim 24^\circ$. The calculated barrier for surface diffusion of a Pt adatom is only 4 kcal/mol, so repulsion between adjacent CO molecules bound to Pt could indeed increase the surface diffusion. However, the residence time of CO on Pt suggests that the CO molecules are extremely mobile, with diffusion constants 40 to 2500 times larger than surface Pt atoms. This mobility suggests that the CO molecules jump between different Pt atoms throughout the simulation. However, they do stay bound to individual Pt atoms for long enough to modify the local energy landscape for the mobile adatoms.

A different interpretation of the above mechanism which takes the large mobility of the CO into account, would be in the destabilization of Pt-Pt interactions due to bound CO. Destabilizing Pt-Pt bonds at the edges could lead to increased step-edge breakup and diffusion. On the bare Pt(557) surface the barrier to completely detach an edge atom is ~ 43 kcal/mol, as is shown in configuration (a) in Figures 2.3 & 2.4. For certain configurations, cases (e), (g), and (h), the barrier can be lowered to ~ 23 kcal/mol by the presence of bound CO molecules. In these instances, it becomes

energetically favorable to roughen the edge by introducing a small separation of 0.5 to 1.0 Å. This roughening becomes immediately obvious in simulations with significant CO populations. The roughening is present to a lesser extent on surfaces with lower CO coverage (and even on the bare surfaces), although in these cases it is likely due to random fluctuations that squeeze out step-edge atoms. Step-edge breakup by direct single-atom translations (as suggested by these energy curves) is probably a worst-case scenario. Multistep mechanisms in which an adatom moves laterally on the surface after being ejected would be more energetically favorable. This would leave the adatom alongside the ledge, providing it with five nearest neighbors. While fewer than the seven neighbors it had as part of the step-edge, it keeps more Pt neighbors than the three neighbors an isolated adatom has on the terrace. In this proposed mechanism, the CO quadrupolar repulsion still plays a role in the initial roughening of the step-edge, but not in any long-term bonds with individual Pt atoms. Higher CO coverages create more opportunities for the crowded CO configurations shown in Figure 2.3, and this is likely to cause an increased propensity for step-edge breakup.

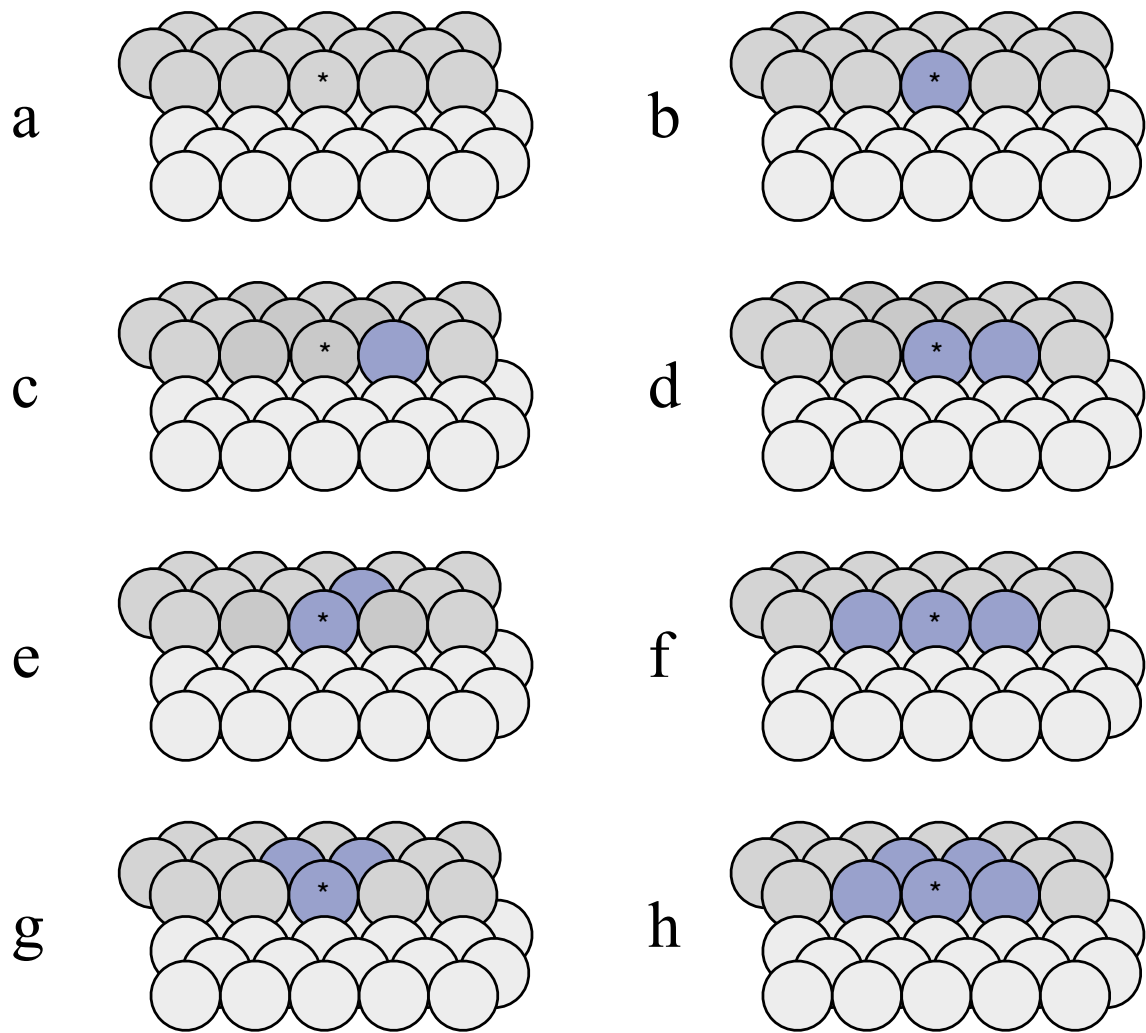


Figure 2.3. Configurations used to investigate the mechanism of step-edge breakup on Pt(557). In each case, the central (starred) atom was pulled directly across the surface away from the step edge. The Pt atoms on the upper terrace are colored dark grey, while those on the lower terrace are in white. In each of these configurations, some of the atoms (highlighted in blue) had CO molecules bound in the vertical atop position. The energies of these configurations as a function of central atom displacement are displayed in Figure 2.4.

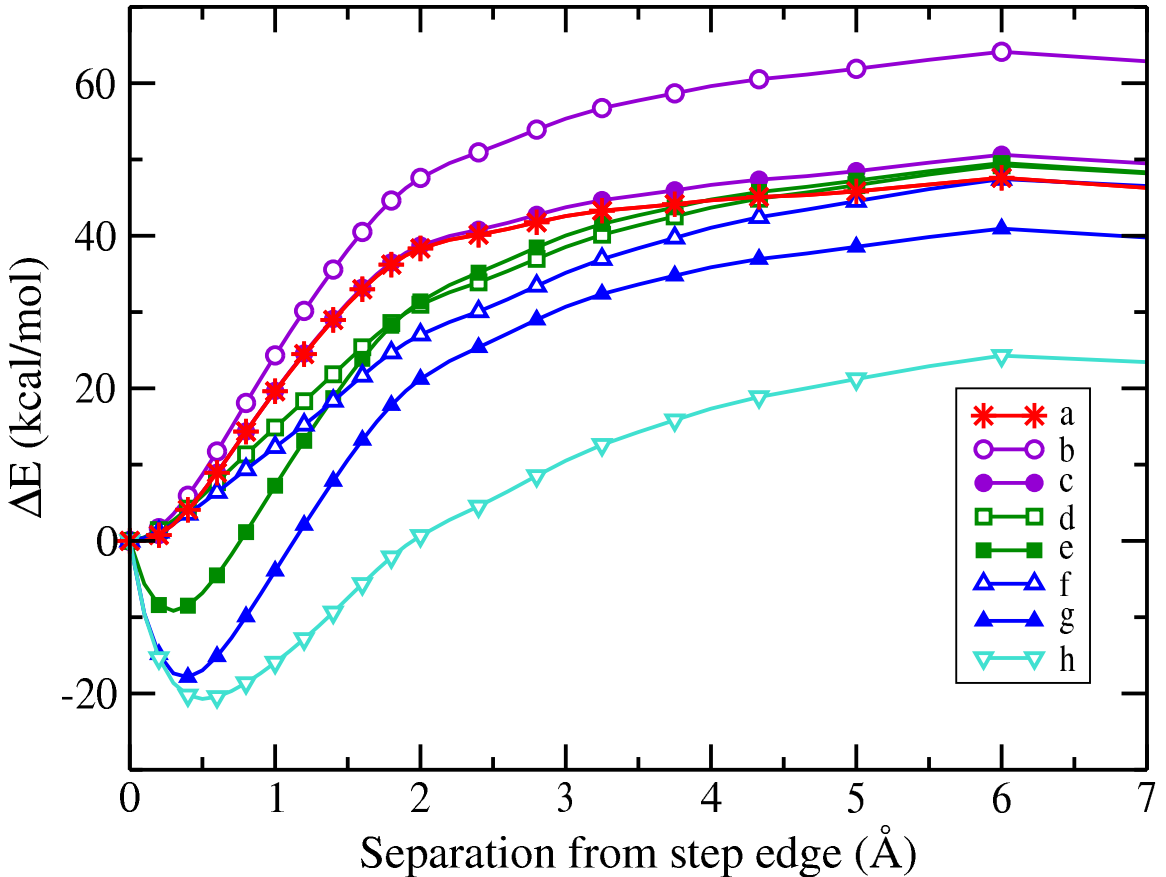


Figure 2.4. Energies for displacing a single edge atom perpendicular to the step edge as a function of atomic displacement. Each of the energy curves corresponds to one of the labeled configurations in Figure 2.3, and the energies are referenced to the unperturbed step-edge. Certain arrangements of bound CO (notably configurations g and h) can lower the energetic barrier for creating an adatom relative to the bare surface (configuration a).

While configurations of CO on the surface are able to increase diffusion and the likelihood of edge wandering, this does not provide a complete explanation for the formation of double layers. If adatoms were constrained to their original terraces then doubling could not occur. A mechanism for vertical displacement of adatoms at the step-edge is required to explain the doubling.

We have discovered one possible mechanism for a CO-mediated vertical displacement of Pt atoms at the step edge. Figure 2.5 shows four points along a reaction coordinate in which a CO-bound adatom along the step-edge “burrows” into the edge and displaces the original edge atom onto the higher terrace. A number of events similar to this mechanism were observed during the simulations. We predict an energetic barrier of 20 kcal/mol for this process (in which the displaced edge atom follows a curvilinear path into an adjacent 3-fold hollow site). The barrier heights we obtain for this reaction coordinate are approximate because the exact path is unknown, but the calculated energy barriers would be easily accessible at operating conditions. Additionally, this mechanism is exothermic, with a final energy 15 kcal/mol below the original $\lambda = 0$ configuration. When CO is not present and this reaction coordinate is followed, the process is endothermic by 3 kcal/mol. The difference in the relative energies for the $\lambda = 0$ and $\lambda = 1$ case when CO is present provides strong support for CO-mediated Pt-Pt interactions giving rise to the doubling reconstruction.

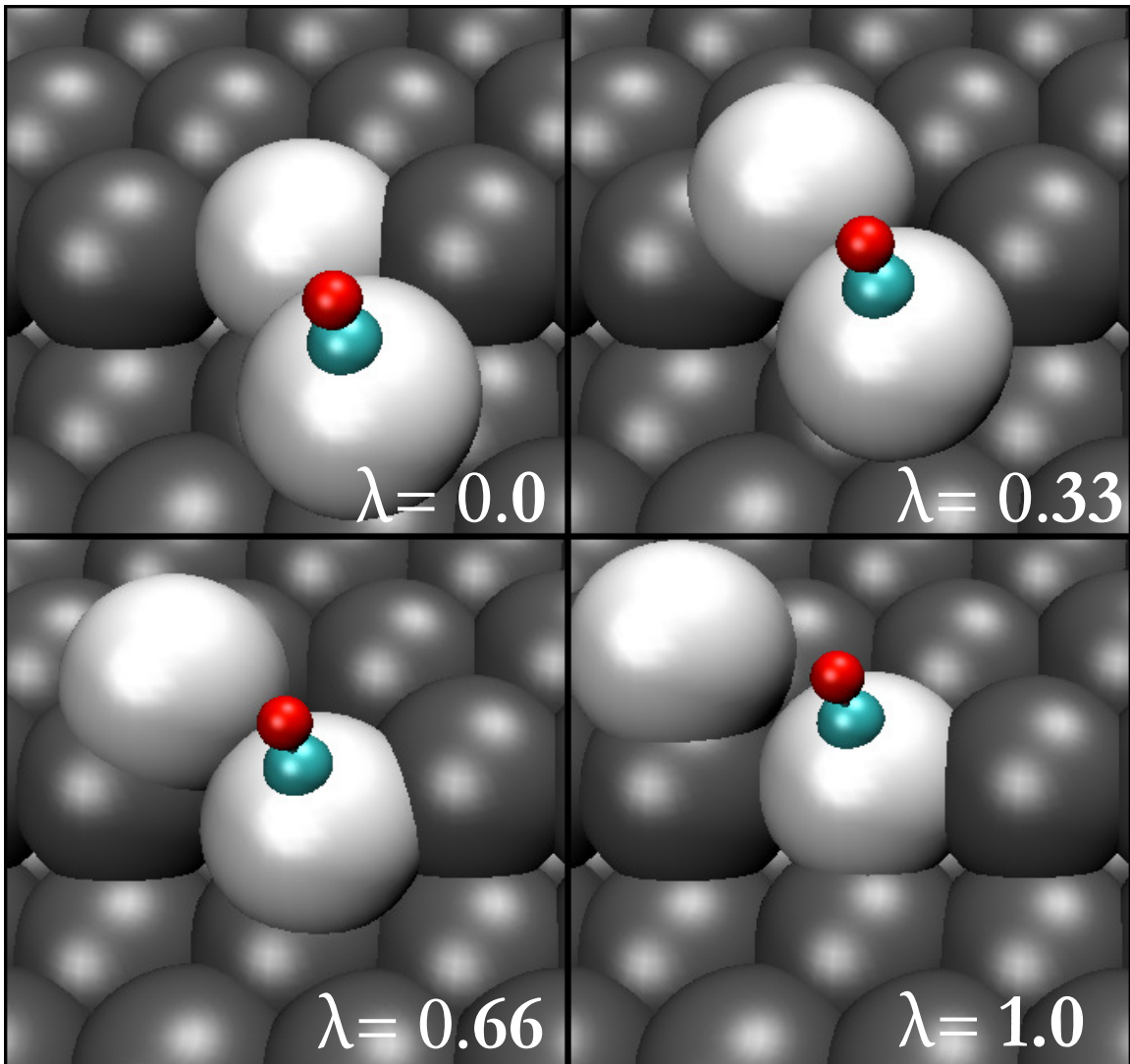


Figure 2.5. Points along a possible reaction coordinate for CO-mediated edge doubling. Here, a CO-bound adatom burrows into an established step edge and displaces an edge atom onto the upper terrace along a curvilinear path. The approximate barrier for the process is 20 kcal/mol, and the complete process is exothermic by 15 kcal/mol in the presence of CO, but is endothermic by 3 kcal/mol without CO.

The mechanism for doubling on the Pt(557) surface appears to require the cooperation of at least two distinct processes. For complete doubling of a layer to occur

there must be a breakup of one terrace. These atoms must then “disappear” from that terrace, either by travelling to the terraces above or below their original levels. The presence of CO helps explain mechanisms for both of these situations. There must be sufficient breakage of the step-edge to increase the concentration of adatoms on the surface and these adatoms must then undergo the burrowing highlighted above (or a comparable mechanism) to create the double layer. With sufficient time, these mechanisms working in concert lead to the formation of a double layer.

2.4.3 CO Removal and double layer stability

Once the double layers had formed on the 50% Pt system, they remained stable for the rest of the simulation time with minimal movement. Random fluctuations that involved small clusters or divots were observed, but these features typically healed within a few nanoseconds. Within our simulations, the formation of the double layer appeared to be irreversible and a double layer was never observed to split back into two single layer step-edges while CO was present.

To further gauge the effect CO has on this surface, additional simulations were run starting from a late configuration of the 50% Pt system that had already formed double layers. These simulations then had their CO molecules suddenly removed. The double layer broke apart rapidly in these simulations, showing a well-defined edge-splitting after 100 ps. Configurations of this system are shown in Figure 2.6. The coloring of the top and bottom layers helps to show how much mixing the edges experience as they split. These systems were only examined for 10 ns, and within that time despite the initial rapid splitting, the edges only moved another few Å apart. It is possible that with longer simulation times, the (557) surface recovery observed by Tao *et al.*¹¹³ could also be recovered.

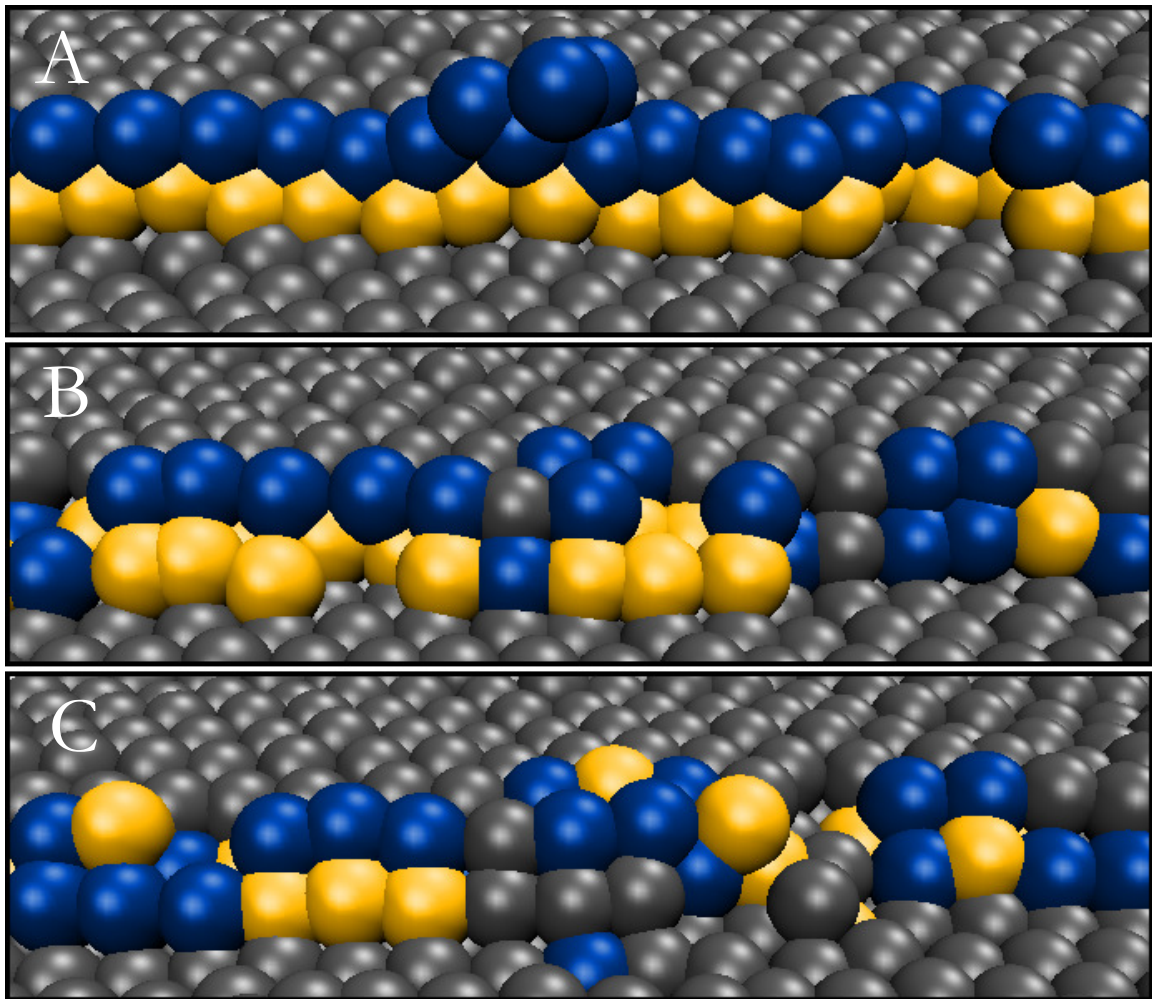


Figure 2.6. Behavior of an established (111) double step after removal of the adsorbed CO: (A) 0 ps, (B) 100 ps, and (C) 1 ns after the removal of CO. Nearly immediately after the CO is removed, the step edge reforms in a (100) configuration, which is also the step type seen on clean (557) surfaces. The step separation involves significant mixing of the lower and upper atoms at the edge.

2.5 Conclusion

The strength and directionality of the Pt-CO binding interaction, as well as the large quadrupolar repulsion between atop-bound CO molecules, help to explain the

observed increase in surface mobility of Pt(557) and the resultant reconstruction into a double-layer configuration at the highest simulated CO-coverages. The weaker Au-CO interaction results in significantly lower adatom diffusion constants, less step-wandering, and a lack of the double layer reconstruction on the Au(557) surface.

An in-depth examination of the energetics shows the important role CO plays in increasing step-breakup and in facilitating edge traversal which are both necessary for double layer formation.

CHAPTER 3

CO-INDUCED ISLAND FORMATION ON PT/PD(557) SURFACE ALLOYS: A MOLECULAR DYNAMICS STUDY

3.1 Introduction

Materials based on metallic Pt and Pd are important catalysts for the oxygen reduction (ORR)^{64, 66, 65} and oxygen evolution reactions (OER).^{105, 90} These reactions are important in proton-exchange membrane (PEM) fuel cells,^{8, 99} as well as in the charging and discharging of Li-air batteries.⁶⁹ Oxide-supported noble metal nanoparticles also play an important role in the water-gas shift reaction.^{11, 62}

However, the expense of Pt metal coupled to the slow kinetics of the ORR on pure Pt or Pt/C systems remain barriers to large-scale implementation of fuel cells. Strategies involving bimetallic particles, surface alloys, and core-shell nanostructures are currently under investigation in hopes of eliminating these barriers.^{37, 38, 54} The coupling of two (or more) components in these structures allows for a large accessible design space for various catalytic properties, whether that be catalytic activity,^{54, 104, 41} thermal stability,^{13, 125, 48} or resistance to deactivation.^{128, 131} Specifically, Pt–Pd nanoparticles have been shown to have increased activity for the ORR reaction,^{64, 66, 99} while Pt–Au nanoparticles were reported as being more stable over repeated potential cycling.¹²⁹

Bimetallic Pt/Pd mixtures also find widespread use in diesel oxidation catalysts (DOC) which complete the oxidation of carbon monoxide and partially-combusted hydrocarbons, and reduce the nitrogen oxides in combustion gases.^{80, 93} Pd is a

particularly useful metal for diesel catalysts because it has a lower intrinsic SO₂ oxidation activity than Pt.⁹³ The Pt/Pd bimetallic catalyst also significantly inhibits sintering of the particles at higher temperatures, relative to pure Pt catalysts.⁸⁰

Catalytic activity is dependent on the exposed structure of Pt in many of these applications. Reconstruction of the exposed Pt can therefore change the effectiveness of a given Pt-M species. Of particular interest in diesel oxidation catalysis is carbon monoxide (CO) and its strong binding affinity for Pt and Pd. Tao *et al.* have shown that the presence of CO can induce reversible surface reconstructions on a stepped Pt(557) surface.¹¹³ Significant experimental and theoretical work has been done to more fully characterize the effect adsorbed CO has on Pt.^{4, 115, 71, 74, 15}

This paper describes an investigation into the effects of carbon monoxide adsorption on surface restructuring of pure Pd(557) and Pt/Pd(557) surface alloys using molecular dynamics simulations. Since the long-time dynamics of the restructuring process are of particular interest, classical force fields which balance computational efficiency against chemical accuracy were employed.

3.2 Methodology

3.2.1 Interaction Potentials

Modeling large metallic interfaces (10^3 - 10^4 atoms) over relatively long time scales (10-100 ns) requires the use of empirical potentials. Cohesive and surface energies in metals are not reproduced with purely pairwise interactions, so a number of empirical potentials have been developed for modeling transition metals. These include the embedded atom method (EAM)³⁵, Finnis-Sinclair,³⁴ and Sutton-Chen-based models like QSC.⁵⁶ These models describe an atom as a positively charged core with a radially-decaying valence electron density. Refinements include angle dependent EAM implementations,³ that treat BCC metals more accurately.

In EAM, the energy for embedding a metallic atom i at a specific location in the system requires the electron density at that location,

$$\rho_i = \sum_{j \neq i} \rho_j(r_{ij}).$$

This density at site i , ρ_i depends on the contributions to the electron density from all other atoms in the system. Here, $\rho_j(r)$ describes the distance dependence of the valence electron distribution of atom j . Atom i 's contribution to the potential energy can then be obtained from an embedding functional, $F_i[\rho_i]$, that depends on ρ_i , as well as from a sum of pairwise interactions,

$$V_i = F[\rho_i] + \sum_{j \neq i} \phi_{ij}(r_{ij})$$

The embedding energy functional is parameterized for each metallic atom type, and depends only on the local electron density, ρ_i . Thus, the cohesive energy for atom i depends on collective contributions from all of the surrounding metal atoms, and is an explicitly non-pairwise additive quantity.

The short-ranged repulsions are treated as a pairwise contribution that models the repulsive overlap of the positively-charged cores. For alloys, mixing rules as outlined by Johnson 52 were used to compute the heterogenous pair potential,

$$\phi_{ab}(r) = \frac{1}{2} \left\{ \left(\frac{\rho_b(r)}{\rho_a(r)} \right) \phi_{aa}(r) + \left(\frac{\rho_a(r)}{\rho_b(r)} \right) \phi_{bb}(r) \right\}$$

One of EAM's strengths is its sensitivity to small changes in local structure which is due to the inclusion of second and third nearest neighbor interactions during parameterization.¹²⁰

In this work, we have employed the embedded atom method (EAM) to describe the Pt and Pd electron densities, embedding functionals, and pair potentials,³⁵ uti-

lizing the Johnson mixing rules for the Pt–Pd cross-interactions.⁵²

The carbon monoxide (CO) self-interactions were modeled using a rigid three-site model developed by Straub and Karplus for studying photodissociation of CO from myoglobin.¹⁰⁶ This model accurately captures the large linear quadrupole (and weak dipole) of the CO molecule. The rigid CO molecules have complete translational and orientational mobility in our simulations.

The Pt–CO interactions have been modified from previous fits⁷⁴ to account for recently-published DFT data.²⁴ This modification yields a slightly weaker Pt–CO binding energy, but maintains the atop site preference. The potential energy for the interaction of one CO molecule with one metal atom,

$$V_{M-CO} = 4\epsilon \left(\left(\frac{\sigma}{r_{M-C}} \right)^{12} - \left(\frac{\sigma}{r_{M-C}} \right)^6 \right) + De^{-2\gamma(r_{M-O}-r_e)}$$

is modeled using a Lennard-Jones interaction between the metal atom (M) and the carbon along with a repulsive Morse potential between the metal atom and the oxygen.

Both the Pd–CO and Pt–CO interaction potentials were parameterized as part of this work. The basic model, using a full Morse potential between the metal and oxygen site and a Lennard-Jones interaction between the metal and the carbon site, was introduced by Korzeniewski *et al.*⁵⁷ One key difference from the potential in Refs.⁵⁷ and our earlier fits in Refs.⁷⁴ is that the M–O bond is modeled here using a purely repulsive Morse potential. The parameters were fit to reflect binding energies and binding site preferences on the M(111) surfaces. The functional forms and the broad repulsive M–O contribution are flexible enough to reproduce the atop preference for Pt–CO as well as the bridge/hollow preference for Pd–CO. Parameters for the potentials are given in Table 3.1 and the calculated binding energies at various binding sites are shown in Table 3.2.

TABLE 3.1
PARAMETERS FOR THE METAL-CO CROSS-INTERACTIONS

| | σ^a | ϵ^b | | r^a | D^b | γ (\AA^{-1}) |
|-------------|------------|--------------|-------------|-------|-------|--------------------------------|
| Pt–C | 1.41 | 45 | Pt–O | 4.4 | 0.05 | 1.8 |
| Pd–C | 1.6 | 40 | Pd–O | 4.95 | 0.05 | 1.45 |

Metal-C interactions are modeled with Lennard-Jones potentials, while the metal-O interactions were fit to Morse potentials.

^a Distances are given in \AA

^b Energies are given in kcal/mol

This Pd–CO model does not have a strong preference for either the bridge or hollow binding sites, so it may overestimate the bridge-site binding at low coverages, but at higher coverages, the experimental situation is somewhat less clear.¹²⁴ Studies using low-energy electron diffraction (LEED) and C–O stretching frequencies of CO bound to Pd(111) suggest that the 3-fold hollow sites are preferred at low coverages,^{10, 18, 81} where it forms a $(\sqrt{3} \times \sqrt{3})R 30^\circ$ pattern. These observations are supported by temperature desorption spectroscopy,⁴³ and infrared absorption spectroscopy¹⁰⁹ where binding energies have been reported to lie between -1.3 and -1.54 eV.

At higher CO coverages (e.g. > 0.5 ML), the preferred binding of CO on Pd(111) appears to be a $c(4 \times 2)$ ordered structure with the CO bound to the bridge sites.¹⁰

Theoretical work by Honkala *et al.*⁴⁶ using DFT with the generalized gradient approximation (GGA) to describe electron exchange correlation and pseudopotentials for the Pd atoms also reported the fcc site as the most favorable binding position with a binding energy of -2.00 eV compared to the bridge site binding energy of -1.83 eV at 0.33 monolayer.

TABLE 3.2
 ADSORPTION ENERGIES FOR A CO MOLECULE AT THE THREE
 PRIMARY BINDING SITES ON M(111)

| | Site | This Model ^a | DFT ^a | Experimental ^a |
|--------------|--------|-------------------------|------------------|----------------------------|
| Pt–CO | atop | -1.47 | -1.4824 | -1.3953, -1.4330, -1.90127 |
| | bridge | -1.13 | -1.4724 | |
| | hollow | -1.02 | -1.4524 | |
| Pd–CO | atop | -1.54 | -1.4446 | |
| | bridge | -1.65 | -1.8346 | |
| | hollow | -1.60 | -1.9946 | -1.30109, -1.4729, -1.5443 |

The energies are obtained using the potentials described in Table 3.1. These values are compared with electronic structure and experimental desorption data when available. Note that the electronic structure values are for surface coverages of *ge* 0.25 ML, and experimental values are (in most cases) extrapolated to zero coverage from desorption energies at higher coverages.

^a All values are in eV

High resolution x-ray photoelectron spectroscopy (XPS) results from Surnev *et al.*¹⁰⁷ confirm that the preferred low coverage (< 0.1 ML) binding site is the fcc hollow, but also suggest a competition between hollow and bridge binding for coverages between 0.1 and 0.32 ML, suggesting similar binding energies for these two sites. Additional DFT calculations from Loffreda *et al.*⁶⁷ suggest that as the coverage increases, the binding energy difference shrinks, as at 0.5 ML the hollow to bridge energy difference is 0.06 eV (-1.85 hollow, -1.79 bridge).

Although the weak preference for hollow vs. bridge sites at low coverage is not captured by the Pd–CO fit, at low temperatures on Pd(111), a 0.5 ML coverage of CO interacting with the potential in Table 3.1 does produce domains with the $c(4 \times 2)$ ordered structure (see supporting information).

Experimental work on CO on Pt(111) using LEED has suggested that the atop binding is 70 meV stronger than the bridge site⁹⁸ and forms a $(\sqrt{3} \times \sqrt{3})R\ 30^\circ$ structure on solely atop sites at low surface coverages.⁵³ Because our Pt-CO model uses relatively long-range repulsive Morse interactions to preserve the CO orientation on the surface, it overestimates the atop binding preference relative to the DFT calculations. However, the model is able to reproduce small domains of the $(\sqrt{3} \times \sqrt{3})R\ 30^\circ$ structures (see supporting information).

3.2.2 (557) Interfaces and surface alloys

The Pd(557) model is contained in an orthorhombic periodic box with dimensions of $55.09 \times 49.48 \times 120\ \text{\AA}$ while the surface alloys (Pt(557) surface layers, with Pd bulk) have dimensions of $54.875 \times 49.235 \times 120\ \text{\AA}$. The Pd system consists of 9 layers of Pd while our surface alloys consist of 7 layers of Pd sandwiched between 2 single layers of Pt. Both the pure Pd slab and the surface alloy systems are $\sim 22\ \text{\AA}$ thick. The lattice constants for Pd and Pt, 3.89 and $3.92\ \text{\AA}$, respectively, result in minimal strain energy in the alloy, and the relaxed geometries of the two interfaces are therefore quite

similar.

The systems are cut from a FCC crystal along the (557) plane, and are rotated so that they are periodic in the x and y directions, exposing (557) facets on both the positive and negative sides of the z -axis of the box.

Simulations of the metal without any adsorbate present were performed at temperatures ranging from 300 to 900 K to establish the stability of the (557) surface without a CO overlayer. The bare systems were run in the canonical (NVT) ensemble at 850 K for 200 ps and the microcanonical (NVE) ensemble for 1 ns, and displayed minimal changes in the (557) structure during this period. This temperature is well below previously simulated melting temperatures for Pt/Pd alloyed nanoparticles in both free and graphite-supported configurations.^{95, 96, 33}

Ten systems were constructed, corresponding to five CO-coverage levels for each metallic system. The number of CO molecules (0, 48, 240, 320, and 480) yield surface coverages of approximately 0, 0.05, 0.25, 0.33, and 0.5 monolayers (ML) assuming that every CO adsorbs on the surface.

Simulation boxes of the same sizes as the metallic systems were constructed with appropriate densities of CO and equilibrated to 850 K. The gas-phase CO and surface simulation boxes were then combined, using a 5 Å cutoff between metallic atoms and CO to prevent overlap. The remaining CO population was further reduced to match the required number for the correct surface coverage. Velocities were resampled from a Boltzmann distribution, and any net linear momentum was subtracted from the entire system. The combined systems were run for 1 ns in the NVT ensemble, before being run in the NVE ensemble for data collection. The CO molecules were initially introduced in the gas phase and were allowed to freely adsorb and migrate on the surface. In most cases, the CO adsorbed on the metal surfaces within the first 100 ps of the initial 1 ns equilibration time.

All of the Pd systems were run in the microcanonical ensemble for a minimum of

40 ns to collect statistics. The Pt/Pd surface alloy systems, which were observed to undergo significant restructuring, were each run for a total simulation time of 113 ns. All simulations were carried out with the open source molecular dynamics package, OpenMD.^{39, 73}

3.2.3 Analysis of surface features and adatom diffusion

To analyze surface domain sizes, the exposed surfaces (both top and bottom of the slabs) were first projected onto 2-dimensional square grids with 1 Å grid spacing. The grid points were assigned “Pt” or “Pd” values based on the identity of the closest surface atom. The grids were then separated into contiguous domains using nearest-neighbor similarity (i.e., the four nearest grid points). The resulting domain areas were averaged over 18 ns windows. A representative grid decomposition is shown in fig. 3.1.

To estimate the surface diffusion constants, we define a mobile atom as one which moves at least 2 Å in any 10 ps window during a 10 ns segment of simulation time. The fraction of exposed surface atoms that met this criteria defines the mobility fraction, f_{mobile} . For the mobile atoms, diffusion constants were calculated in 10 ns windows to follow changes in adatom transport after the initial exposure to CO.

3.3 Results

3.3.1 Structural changes

On Pt(557), we previously observed CO-induced restructuring into relatively clean double-layer structures.⁷⁴ For the pure Pd(557) studied here, the (557) facet retains the (111) plateaus and (100) steps with only minimal adatom movement, and with almost no surface reconstruction. Higher CO coverages appear to have minimal effect (and may even stabilize the steps) when compared with the bare Pd(557) systems.

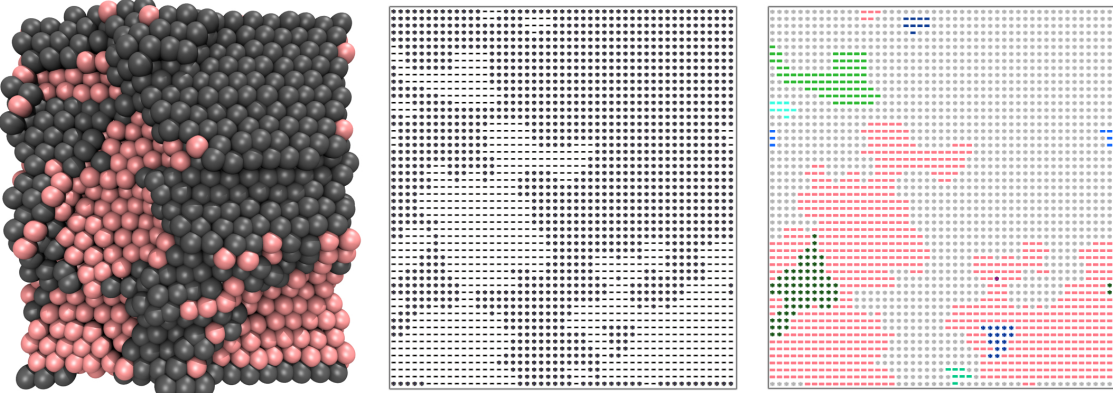


Figure 3.1. Analysis of the surface alloy to find surface domain sizes was carried out by mapping the surface composition (left) onto 1 Å spaced grid points (center). Contiguous domains were identified and have been shown in distinct colors (right), and the distribution of domain areas was collected over 18 ns time windows.

The Pt-coated Pd surface alloy exhibits a CO-induced speedup of Pt-adatom diffusion, as well as a large-scale restructuring of the well-ordered surface into Pt-rich islands. This surface will therefore be the focus of most of our analysis.

Figure 3.2 shows representative configurations of the various systems after significant exposure to the CO. We see that the Pd system highlighted in panel (a) has undergone no surface restructuring. The other panels highlight the effect of varying CO concentrations on the surface alloys, which do exhibit structural reorganization.

3.3.2 Transport of surface metal atoms

Figure 3.2 suggests that there is limited to no mobility on the pure Pd systems. Analysis of the surface atom mobility showed that fewer than 6% of the surface Pd atoms made $> 2 \text{ \AA}$ hops in any 10 ps window during the entire 40 ns run. As most of these atoms immediately hopped back to their starting points, surface diffusion constants on Pd(557) are as close to zero as can be safely estimated.

However, there is significant movement of surface Pt in the alloy systems, and the

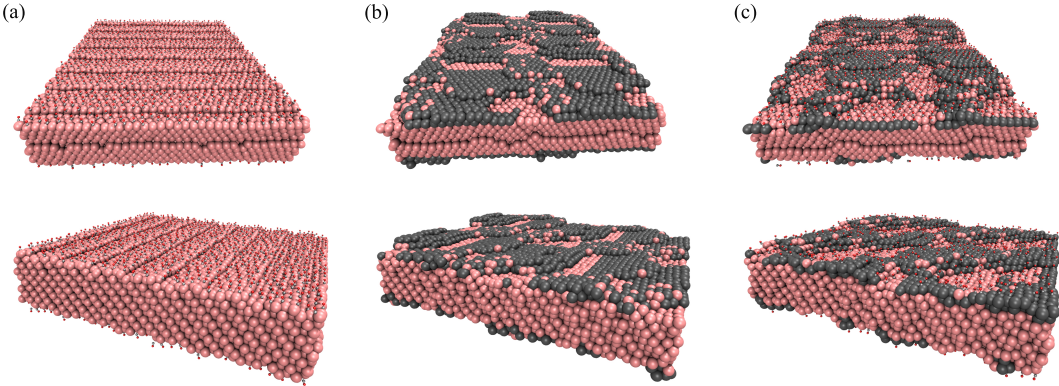


Figure 3.2. Snapshots of some of the simulated systems highlighting the (557) step edges (top) along with a diagonal view (bottom). System (a) is the pure Pd (557) ~ 40 ns after being dosed with 0.5 ML of CO. System (b) is the bare surface alloy after ~ 110 ns at 850 K, while (c) is the surface alloy ~ 110 ns after exposure to 0.5 ML of CO. Pt atoms are shown in gray, Pd in pink, while the adsorbed CO molecules are shown in silver / red.

mobility of the surface Pt layer increases with increasing CO coverage. The initial 50 ns of exposure is far from equilibrium, and adatom diffusion constants stabilize after this 50 ns period. The diffusion constants shown in Table 3.3 are calculated from the last (equilibrated) 60 ns of each simulation. The fraction of mobile surface atoms grows linearly with increasing CO coverage from 27% of the bare metal surface with no CO overlayer to 33% of the surface metal atoms under 0.5 ML of CO.

3.3.3 Pt island formation on the Pt/Pd alloy

At the beginning of the simulations, the surface layer of Pt made up one domain of $\sim 2625 \text{ \AA}^2$. In all simulations, this domain broke up relatively quickly and was matched by a growth in the number and size of Pd domains. The presence of CO in the system increased the clustering of the Pt domains, with a concomitant exposure of the underlying Pd.

The structural reconstructions that occur for the surface alloy are influenced by

TABLE 3.3
 FRACTION OF MOBILE PT SURFACE ATOMS AND THEIR
 SURFACE DIFFUSION

| CO Coverage | f_{mobile} | D ($\text{\AA}^2/\text{ns}$) |
|-------------|---------------------|----------------------------------|
| 0.00 | 0.27(1) | 1.1(3) |
| 0.05 | 0.28(2) | 1.2(3) |
| 0.25 | 0.30(2) | 1.3(3) |
| 0.33 | 0.37(2) | 1.7(3) |
| 0.50 | 0.33(3) | 1.0(2) |

The fraction of mobile Pt surface atoms (f_{mobile}) and surface diffusion constants (D) for the surface alloys as a function of the CO coverage

Uncertainties in the last digit are shown in parentheses

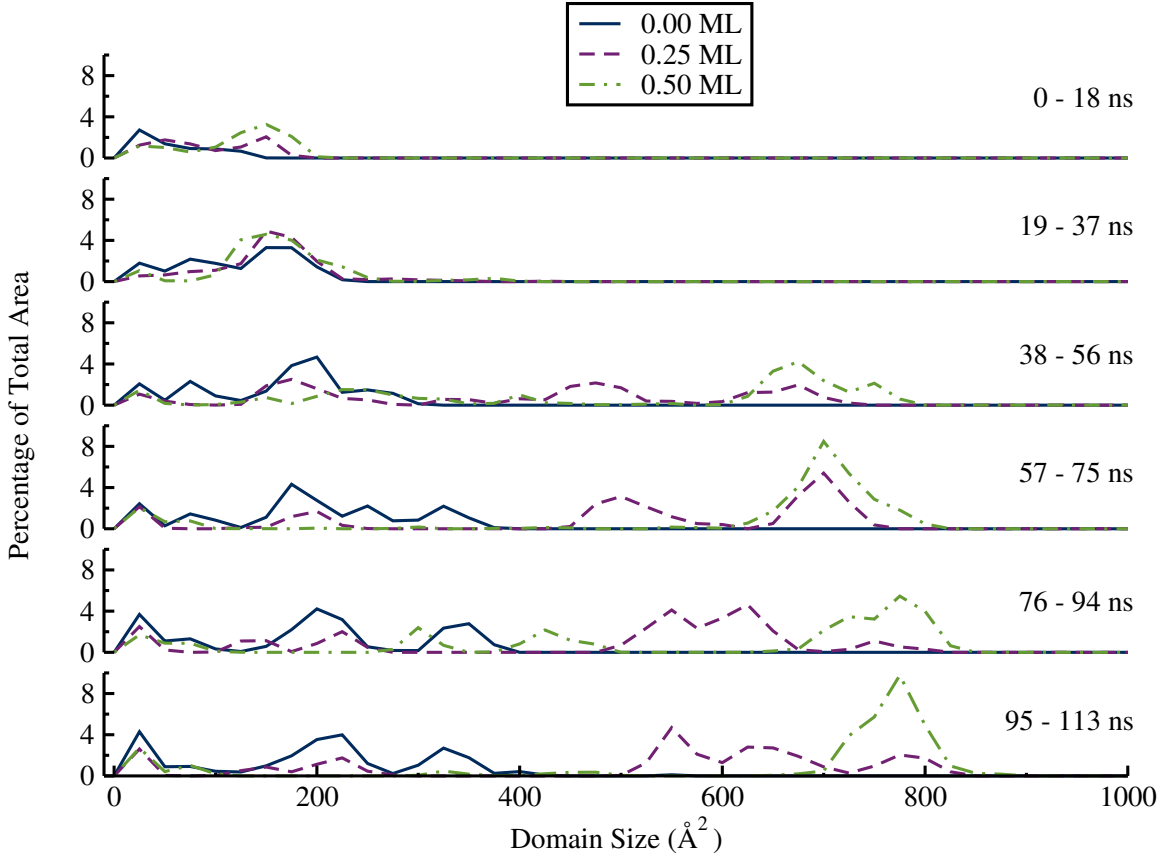


Figure 3.3. Distributions of Pd domain sizes at different CO coverages and at different times after exposure to CO.

the presence of the CO adsorbate. In Figure 3.3, the area of exposed Pd increases both over time, and as a function of CO coverage. The presence of CO increases exposure of the underlying Pd, as measured by the number and sizes of exposed Pd domains. Without CO exposure, the bare Pt/Pd surface does undergo some restructuring at 850 K, although both the rate and extent is significantly smaller than in the 0.25 and 0.50 monolayer (ML) systems.

The appearance of Pd from the bulk layers on the surface requires a simultaneous reduction in the surface area of the outer Pt skin. Two scenarios could explain the reduction of exposed Pt: either the Pt atoms are being buried under the Pd bulk, or islands of Pt are forming on top of the Pd surface.

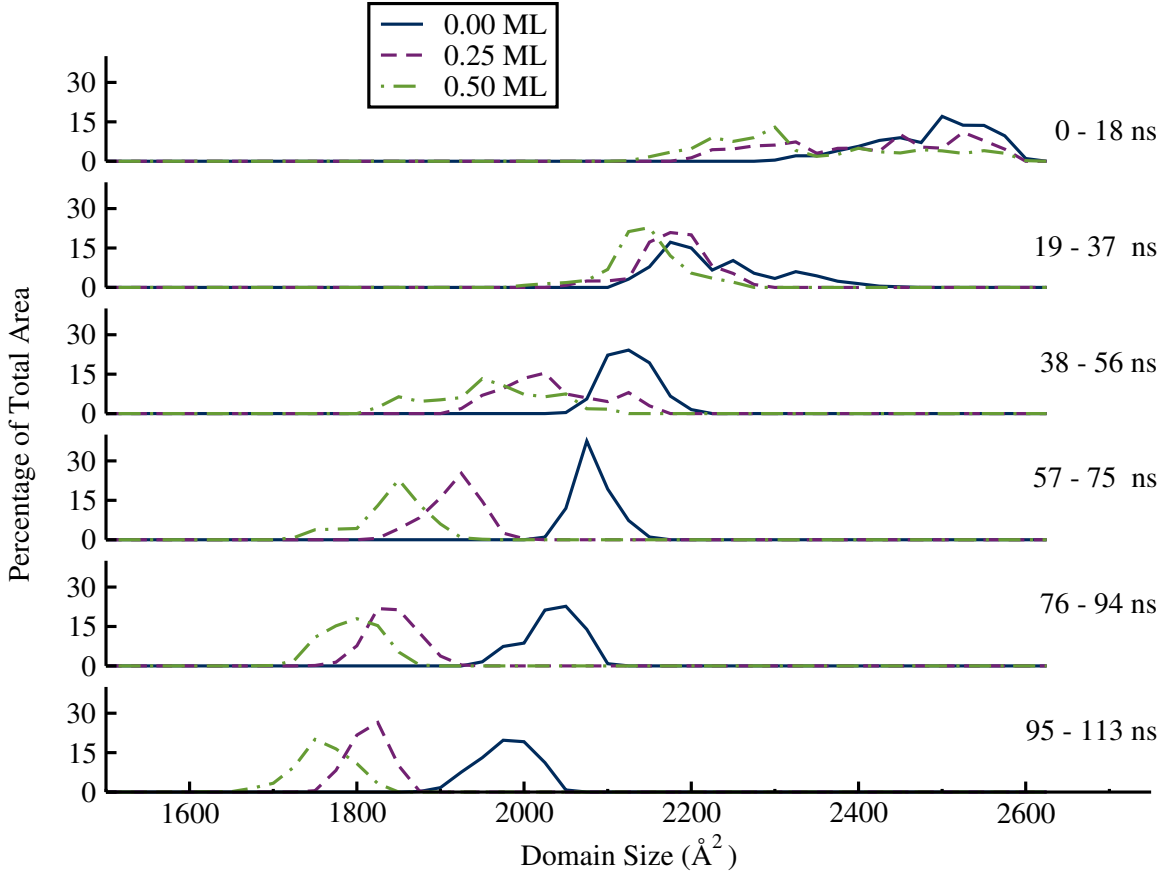


Figure 3.4. Distributions of Pt domain sizes at different CO coverages and at different times after exposure to CO.

Both mechanisms would explain the decreased Pt surface area (see Fig. 3.4). To discern which of these mechanisms is taking place, the identity of nearest metal atom neighbors can be tabulated as a function of time of exposure to CO. Single-layer Pt skins have atoms with 6 Pt nearest neighbors. Islands of Pt require the presence of Pt atoms with 7-9 Pt nearest neighbors. In figure 3.5, we see an increase in Pt population with 9 Pt nearest neighbors along with the simultaneous decrease in Pt atoms with only 6 Pt nearest neighbors. This is evidence for the formation of multi-layer Pt features since single layers of Pt are restricted to having 6 Pt nearest neighbors.

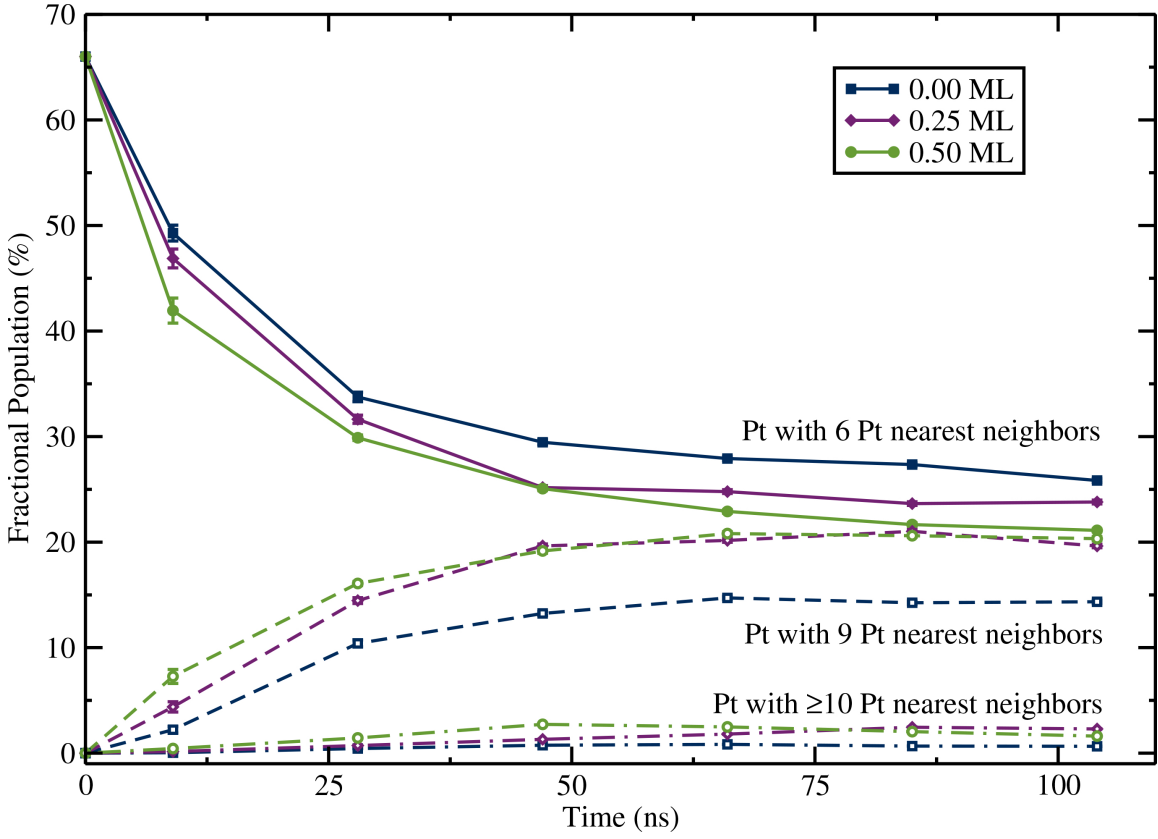


Figure 3.5. Population of Pt atoms with either 6 (solid), 9 (dashed), or ≥ 10 (dot-dashed) Pt nearest neighbors averaged over 18 ns blocks of time. At $t = 0$, the majority ($2/3$) of Pt is located in the (111) plateaus where the number of Pt nearest neighbors is 6. The remaining Pt is located at step edges, with a nearest neighbor Pt count of 5.

Although it is not shown in Figure 3.4, there is an additional small peak in the Pt graphs around 0-100 Å, corresponding to 1 to 2 atom clusters of Pt embedded in the Pd matrix. A figure showing the full scale of domain sizes is supplied in the supporting information. The integrated area of Pd surface coverage for each time window is shown in Table 3.4.

The presence of CO therefore appears to facilitate the clustering of Pt into smaller domains by forming multilayer features which leads to a reduction of Pt surface coverage and concomitant increased exposure of the underlying Pd. We note that

TABLE 3.4
CHANGE IN PD SURFACE COVERAGE OVER SIMULATION

| CO coverage | 0-18 ns | 19-37 ns | 38-56 ns | 57-75 ns | 76-94 ns | 95-113 ns |
|-------------|---------|----------|----------|----------|----------|-----------|
| 0.00 | 6.6 | 16.2 | 20.1 | 21.7 | 23.5 | 25.2 |
| 0.05 | 8.0 | 15.8 | 20.2 | 25.1 | 27.6 | 30.9 |
| 0.25 | 8.5 | 17.3 | 23.7 | 27.8 | 30.5 | 31.0 |
| 0.33 | 8.8 | 17.8 | 21.9 | 26.2 | 30.3 | 35.4 |
| 0.50 | 11.8 | 19.2 | 25.9 | 29.8 | 31.1 | 32.6 |

The amount of Pd surface coverage is shown as a percentage of the total surface area. The individual data points are averaged over 18 nanosecond blocks of time.

nearest-neighbor population analysis provides information similar to the information one might obtain from an XAFS experiment, which could make this phenomenon experimentally observable.

The slower restructuring observed in the bare metal system suggests that the relative surface energies of the two metals provides the driving force for the restructuring, while the CO significantly speeds up the effects (and may help to catalyze the process at lower temperatures).

Because many of the changes, both in domain size and in Pt-atom neighborship slow after 50 ns, this timescale appears to indicate the onset of stable surface structures. The presence of adsorbed CO hastens the onset of this quasi-equilibrium, although there is insufficient data to predict rates from our simulations.

3.4 Discussion

3.4.1 Structural changes

In our previous work on Pt(557) surfaces,⁷⁴ the surface exhibited a CO-induced structural transformation from single steps to double steps, where the (111) plateaus effectively doubled in size. The step coherence and orientation was preserved following the transformation. In the alloy case studied here, the Pt atoms start to cluster, breaking up the steps and causing significant disorder on the surface. We note, however, that the underlying Pd maintains the step-like structures of the (557) interface. A figure showing how the underlying Pd(557) survives the surface island formation is supplied in the supporting information.

The EAM potential predicts surface energies for Pd (111), (100), and (110) facets that are roughly 84% of the surface energies for the same facets on bare Pt.³⁵ Although the absolute EAM surface energies differ significantly from experimental values, the Pd:Pt surface energy ratio is similar to experimental results.^{117, 21} All-electron full potential linearized augmented plane-wave (FP-LAPW) calculations have also yielded a 0.84:1 ratio between the Pd:Pt (111) surface energies.¹⁰³ The (557) interface has broad steps of exposed (111), so we expect the ratio between the Pd:Pt (557) surface energies to also fall close to this 0.84:1 ratio.

Because Pt has a higher surface energy, the alloy system will experience a driving force towards arrangements that minimize the Pt surface area. Although the Pt island formation appears to be accelerated by the presence of adsorbed CO, the relationship between CO-adsorption and the surface energies was not initially clear. In the sections below, we discuss the effects that the bound-CO has on step edge stability and surface diffusion.

We note that on Pt(557), CO aids in double layer formation by lowering the barrier for an adatom on the lower plateau to burrow into a nearby step edge.⁷⁴

This burrowing lifts one of the step edge atom onto the step above. On the alloy surface, this same mechanism can explain the thickening of the Pt island layers that is required by the 9-nearest neighbor clustering in fig.3.5.

3.4.2 Surface adatom formation

There is limited movement of Pd in all of the systems we examined. Inversions, where Pd and Pt atoms are swapped between surface and subsurface layers, were observed only rarely in the Pd/Pt shell, and overall the Pd is largely stationary.

The binding preference of CO for bridge and hollow sites on the Pd surface plays a stabilizing role for step edges. The Pd(557) systems show a decrease in surface roughening at higher CO coverages. Figure 3.6 shows an analysis of the energy required to move a step-edge atom into an adatom position on the step below. In this figure, one step-edge Pd atom is pulled across the surface perpendicular to the step edge. Bridging CO molecules adsorbed to neighbors of an edge atom will raise the barrier that must be overcome to form a free adatom (see curves B and C in Fig. 3.6).

If the step-edge atom is directly bound to CO as one part of a bridge or hollow site, there is an even larger energetic barrier to overcome before the adatom can be released (see curves D, E, and F in Fig. 3.6).

This CO-induced step stabilization is significantly different from the Pt–CO interaction which favors the atop binding position. In the Pt–CO case, additional bound CO on the surface and has previously been shown to facilitate surface roughening.⁷⁴ The Pt–CO potential in table 3.1 has been altered from the original parameters in Ref. 74, and figure 3.7 shows that for the new potential, adsorbed CO can also disrupt step edges, providing an energetic benefit to increasing the exposed Pt surface area.

Based on the curves in Figs. 3.6 and 3.7, the CO adsorbates appear to increase the

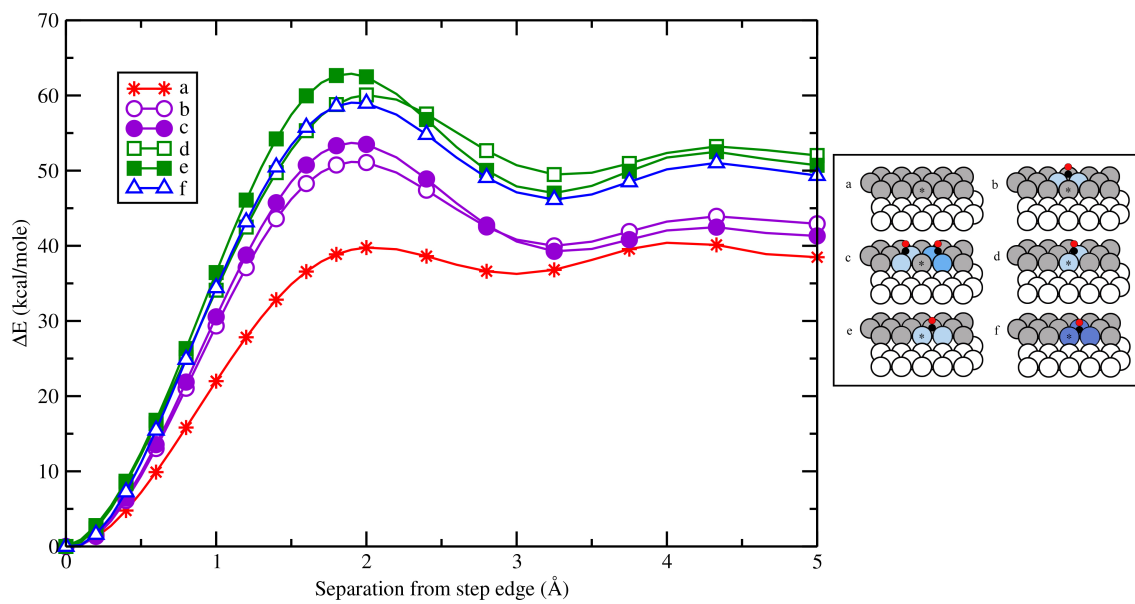


Figure 3.6. The relative energies for moving a Pd atom (marked with an asterisk) perpendicular to a (557) step edge. This atom is translated across the bare Pd surface in curve A. The presence of one or two CO molecules bound in bridge sites near the edge significantly stabilizes the edge atom (curves B and C). If CO is bound to the edge atom in either a bridge (curves D and E) or hollow (curve F) site, the barrier is increased.

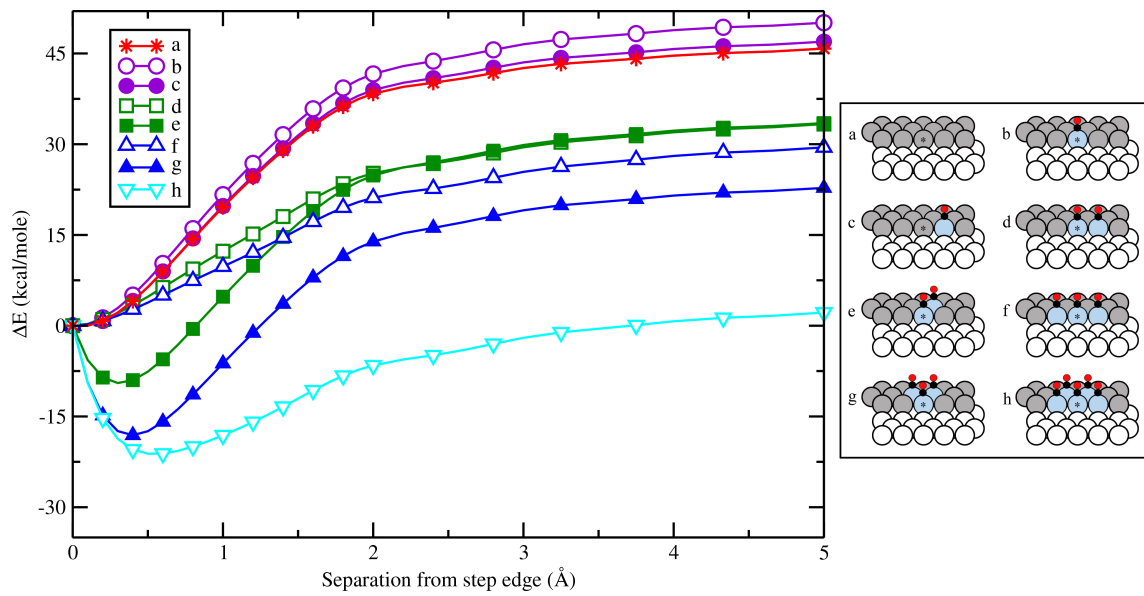


Figure 3.7. The relative energies for moving a step-edge Pt atom (marked with an asterisk) perpendicular to a (557) step edge. As in figure 3.6, the bare surface is shown in curve A. The presence of atop-bound CO molecules on the edge atom and at nearby sites can lower the energy for adatom formation (e.g. curves E, G, and H).

surface energy of stepped Pd surfaces and to lower the surface energy of equivalent Pt surfaces. Therefore, a kinetic mechanism seems to be the most reasonable explanation for the enhancement of island formation. By effectively lowering the surface energy of the Pt, the bound CO increases Pt-atom mobility. Once the mobile Pt atoms find nearby islands, the surface energies still favor compact structures, and the islands can grow more rapidly. These islands then sit on top of a CO-stabilized Pd substrate. Additionally, since the modeled Pd–CO binding is somewhat stronger than Pt–CO, island formation exposes more of the Pd substrate for energetically-favorable gas adsorption.

3.5 Summary

Our primary conclusion is that the presence of chemisorbed carbon monoxide can speed up the formation of Pt islands on the surface of a catalytically-interesting alloy, but that this effect is largely kinetic in nature. The bare Pd surface is stabilized by the CO adsorbate, while stepped Pt surfaces are roughened and destabilized by the presence of the same molecule. The larger surface energies of Pt relative to Pd already favor the segregation of Pt into compact domains. At elevated temperatures, we observe the beginnings of island formation even without the CO adsorbate on the surface, which indicates that thermodynamics favors island formation on this surface.

The energy profiles for step-edge adatom formation in the presence of adsorbed CO (see figs. 3.6 and 3.7) would seem to bring the relative surface energies closer together in the presence of the adsorbed CO. Thermodynamically, this should destabilize Pt islands, so our observation that the 0.5 ML CO speeds up the island-formation process appears to be due largely to kinetics. The lower barriers for Pt-adatom formation effectively speed up the surface diffusion of Pt. Previous work on Pt(557) surfaces showed that CO also lowers the barrier for a step-burrowing mechanism that can increase the thickness of Pt surface layers.⁷⁴

We note that there are other catalytically-active Pt-alloys (notably PtNi_3 and PtNi_6 nanoparticles) that display dealloying of Pt upon electrochemical cycling.¹¹⁶ In analogy to the Pd alloy studied here, the binding of CO on Ni(111) also prefers hollow sites in preference to atop locations.¹² However, the surface energies of Ni are close to those of Pt, so it is not clear if our conclusions about the Pd/Pt alloy would apply to this system. Further research on these alloys would require adapting the M–CO models in order to predict whether carbon monoxide would be a generally effective tool for concentrating catalytically-active Pt sites on surface alloys.

CHAPTER 4

EFFECTS OF STEP-TYPE ON THE CO-INDUCED SURFACE RECONSTRUCTIONS OF PT(557)/(112)/(321)/(765) FACETS

CHAPTER 5

DEVELOPMENT OF A MULTIPLE-MINIMA FLUCTUATING CHARGE (MM-FLUCQ) POTENTIAL

CHAPTER 6

SUMMARY

BIBLIOGRAPHY

1. E. Ahmed, J. Akhter, and M. Ahmad. Molecular dynamics study of thermal properties of noble metals. *Computational Materials Science*, 31:309–316, 2003.
2. M. M. G. Alemany, C. Rey, and L. J. Gallego. Transport coefficients of liquid transition metals: A computer simulation study using the embedded atom model. 109:5175–5176, 1998.
3. M. I. Baskes. Application of the embedded-atom method to covalent materials: A semiempirical potential for silicon. *Phys. Rev. Lett.*, 59:2666–2669, Dec 1987. doi: 10.1103/PhysRevLett.59.2666. URL <http://link.aps.org/doi/10.1103/PhysRevLett.59.2666>.
4. J. Batteas, J. Dunphy, G. Somorjai, and M. Salmeron. Coadsorbate induced reconstruction of a stepped Pt(111) surface by sulfur and CO: A novel surface restructuring mechanism observed by scanning tunneling microscopy. *Phys. Rev. Lett.*, 77(3):534–537, 1996. ISSN 0031-9007. doi: 10.1103/PhysRevLett.77.534.
5. C. S. Becquart, D. Kim, J. A. Rifkin, and P. C. Clapp. Fracture properties of metals and alloys from molecular-dynamics simulations. *Materials Science and Engineering A-Structural Materials Properties Microstructure and Processing*, 170:87–94, 1993.
6. A. B. Belonoshko, R. Ahuja, O. Eriksson, and B. Johansson. Quasi *ab initio* molecular dynamic study of Cu melting. 61:3838–3844, 2000.
7. C. Bhattacharya, M. Srivastava, and S. Menon. Melting curves of fcc-metals by cell-theory. *Physica B: Condensed Matter*, 406:4035–4040, July 2011.
8. S. T. Bliznakov, M. B. Vukmirovic, L. Yang, E. A. Sutter, and R. R. Adzic. Pt monolayer on electrodeposited Pd nanostructures: Advanced cathode catalysts for PEM fuel cells. *J. Electrochem. Soc.*, 159(9):F501–F506, 2012. doi: 10.1149/2.006209jes. URL <http://jes.ecsdl.org/content/159/9/F501.abstract>.
9. P. E. Blöchl. Projector augmented-wave method. 50(24):17953–17979, Dec 1994. doi: 10.1103/PhysRevB.50.17953.
10. A. M. Bradshaw and F. M. Hoffmann. The chemisorption of carbon monoxide on palladium single crystal surfaces: Ir spectroscopic evidence for localised site adsorption. *Surf. Sci.*, 72(3):513–535, 4 1978. doi: [http://dx.doi.org/10.1016/0039-6081\(78\)90004-7](http://dx.doi.org/10.1016/0039-6081(78)90004-7).

- 1016/0039-6028(78)90367-9. URL <http://www.sciencedirect.com/science/article/pii/0039602878903679>.
11. T. Bunluesin, R. Gorte, and G. Graham. Studies of the water-gas-shift reaction on ceria-supported pt, pd, and rh: Implications for oxygen-storage properties. *Appl. Catal., B*, 15(1–2):107 – 114, 1998. ISSN 0926-3373. doi: [http://dx.doi.org/10.1016/S0926-3373\(97\)00040-4](http://dx.doi.org/10.1016/S0926-3373(97)00040-4). URL <http://www.sciencedirect.com/science/article/pii/S0926337397000404>.
 12. J. C. Campuzano and R. G. Greenler. The adsorption sites of CO on Ni(111) as determined by infrared reflection-absorption spectroscopy. *Surf. Sci.*, 83(1):301 – 312, 1979. ISSN 0039-6028. doi: [http://dx.doi.org/10.1016/0039-6028\(79\)90495-3](http://dx.doi.org/10.1016/0039-6028(79)90495-3). URL <http://www.sciencedirect.com/science/article/pii/0039602879904953>.
 13. A. Cao and G. Veser. Exceptional high-temperature stability through distillation-like self-stabilization in bimetallic nanoparticles. *Nat Mater*, 9(1):75–81, 01 2010. URL <http://dx.doi.org/10.1038/nmat2584>.
 14. R. Car and M. Parrinello. Unified approach for molecular-dynamics and density-functional theory. 55(22):2471–2474, 1985. ISSN 0031-9007. doi: 10.1103/PhysRevLett.55.2471.
 15. S. Carenco. Carbon monoxide-induced dynamic metal-surface nanostructuring. *Chem.-Eur. J.*, 20(34):10616–10625, 2014. ISSN 1521-3765. doi: 10.1002/chem.201403140. URL <http://dx.doi.org/10.1002/chem.201403140>.
 16. N. Chetty and V. W. Couling. Measurement of the electric quadrupole moment of co. *J. Chem. Phys.*, 134:164307, April 2011.
 17. Y. Chui and K. Chan. Analyses of surface and core atoms in a platinum nanoparticle. 5:2869–2874, 2003. doi: DOI10.1039/b302122j.
 18. H. Conrad, G. Ertl, and J. Küppers. Interactions between oxygen and carbon monoxide on a pd(111) surface. *Surf. Sci.*, 76(2):323–342, 9 1978. doi: [http://dx.doi.org/10.1016/0039-6028\(78\)90101-2](http://dx.doi.org/10.1016/0039-6028(78)90101-2). URL <http://www.sciencedirect.com/science/article/pii/0039602878901012>.
 19. M. S. Daw. Model of metallic cohesion: The embedded-atom method. 39:7441–7452, 1989.
 20. M. S. Daw and M. I. Baskes. Embedded-atom method: Derivation and application to impurities, surfaces, and other defects in metals. 29(12):6443–6453, 1984.
 21. F. R. De Boer, R. Boom, W. C. M. Mattens, A. R. Miedema, and A. K. Niessen. *Cohesion in Metals: Transition Metal Alloys*, volume 1 of *Cohesion and Structure*. Elsevier, Amsterdam, 1988.

22. J. Derouin, R. G. Farber, S. Heslop, and D. R. Killelea. Formation of surface oxides and ag₂O thin films with atomic oxygen on Ag(111). *Surface Science*, (0):–, 2015. ISSN 0039-6028. doi: <http://dx.doi.org/10.1016/j.susc.2015.07.003>. URL <http://www.sciencedirect.com/science/article/pii/S0039602815001958>.
23. P. Deshlahra, E. E. Wolf, and W. F. Schneider. A periodic density functional theory analysis of CO chemisorption on Pt(111) in the presence of uniform electric fields. *J. Phys. Chem. A*, 113:4125, February 2009.
24. P. Deshlahra, J. Conway, E. E. Wolf, and W. F. Schneider. Influence of dipole-dipole interactions on coverage-dependent adsorption: Co and NO on Pt(111). *Langmuir*, 28:8408, April 2012.
25. P. Deshlahra, J. Conway, E. E. Wolf, and W. F. Schneider. Influence of dipole-dipole interactions on coverage-dependent adsorption: Co and NO on Pt(111). *Langmuir*, 28(22):8408–8417, 2012. doi: 10.1021/la300975s. URL <http://dx.doi.org/10.1021/la300975s>. PMID: 22545625.
26. G. S. Elliott and D. R. Miller. *Helium Scattering from CO Adsorbed on Au(111)*, volume 1 of *Proc. 14th Int. Symp. on Rarefied Gas Dynamics*, pages 349–58. University of Tokyo Press, 1984.
27. F. Ercolelli, M. Parrinello, and E. Tosatti. Simulation of gold in the glue model. *Philosophical Magazine a*, 58:213–226, 1988.
28. G. Ertl. Reactions at surfaces: From atoms to complexity (nobel lecture). *Angewandte Chemie-International Edition*, 47(19):3524–3535, 2008.
29. G. Ertl and J. Koch. Adsorption von CO auf einer palladium(111)-oberfläche. *Z. Naturforsch., A: Phys. Sci.*, 25:1906, 1970.
30. G. Ertl, M. Neumann, and K. Streit. Chemisorption of CO on the Pt(111) surface. *Surface Science*, 64:393, January 1977.
31. P. J. Feibelman and et al. The CO/Pt(111) puzzle. *J. Phys. Chem. B*, 105: 4018–4025, 2001.
32. C. J. Fennell and J. D. Gezelter. Is the Ewald summation still necessary? pairwise alternatives to the accepted standard for long-range electrostatics. *J. Chem. Phys.*, 124:234104, June 2006.
33. C. Fernández-Navarro and S. Mejía-Rosales. Molecular dynamics of free and graphite-supported Pt-Pd nanoparticles. *Advances in Nanoparticles*, 2(4):323–328, 2013.
34. M. W. Finnis and J. E. Sinclair. A simple empirical n-body potential for transition-metals. *Phil. Mag. A*, 50:45–55, 1984.

35. S. M. Foiles, M. I. Baskes, and M. S. Daw. Embedded-atom-method functions for the fcc metals Cu, Ag, Au, Ni, Pd, Pt, and their alloys. *Phys. Rev. B*, 33(12):7983–7991, June 1986.
36. S. M. Foiles, M. I. Baskes, and M. S. Daw. Embedded-atom-method functions for the fcc metals Cu, Ag, Au, Ni, Pd, Pt, and their alloys. 33(12):7983, 1986.
37. F. Gao, Y. Wang, and D. W. Goodman. CO oxidation over AuPd(100) from ultrahigh vacuum to near-atmospheric pressures: CO adsorption-induced surface segregation and reaction kinetics. *J. Phys. Chem. C*, 113(33):14993–15000, 2009. doi: 10.1021/jp9053132. URL <http://dx.doi.org/10.1021/jp9053132>.
38. F. Gao, Y. Wang, and D. W. Goodman. CO oxidation over AuPd(100) from ultrahigh vacuum to near-atmospheric pressures: The critical role of contiguous Pd atoms. *J. Am. Chem. Soc.*, 131(16):5734–5735, 2009. doi: 10.1021/ja9008437. URL <http://dx.doi.org/10.1021/ja9008437>.
39. J. D. Gezelter, J. Michalka, S. Kuang, J. Marr, K. Stocker, C. Li, C. F. Vardeman, T. Lin, C. J. Fennell, X. Sun, K. Daily, Y. Zheng, and M. A. Meineke. OpenMD, an Open Source Engine for Molecular Dynamics. Available at <http://openmd.org>.
40. P. Giannozzi, S. Baroni, N. Bonini, M. Calandra, R. Car, C. Cavazzoni, D. Ceresoli, G. L. Chiarotti, M. Cococcioni, I. Dabo, A. Dal Corso, S. de Gironcoli, S. Fabris, G. Fratesi, R. Gebauer, U. Gerstmann, C. Gougaoussis, A. Kokalj, M. Lazzeri, L. Martin-Samos, N. Marzari, F. Mauri, R. Mazzarello, S. Paolini, A. Pasquarello, L. Paulatto, C. Sbraccia, S. Scandolo, G. Sclauzero, A. P. Seitsonen, A. Smogunov, P. Umari, and R. M. Wentzcovitch. Quantum espresso: a modular and open-source software project for quantum simulations of materials. *Journal of Physics: Condensed Matter*, 21(39):395502 (19pp), 2009. URL <http://www.quantum-espresso.org>.
41. X.-K. Gu, B. Liu, and J. Greeley. First-principles study of structure sensitivity of ethylene glycol conversion on platinum. *ACS Catalysis*, 5(0):2623–2631, 2015. doi: 10.1021/cs5019088. URL <http://dx.doi.org/10.1021/cs5019088>.
42. R. Guidelli and W. Schmickler. Recent developments in models for the interface between a metal and an aqueous solution. 45(15-16):2317–2338, 2000. ISSN 0013-4686. doi: 10.1016/S0013-4686(00)00335-2.
43. X. Guo and J. T. Yates. Dependence of effective desorption kinetic parameters on surface coverage and adsorption temperature: CO on Pd(111). *J. Chem. Phys.*, 90(11):6761, 1989. ISSN 00219606. doi: 10.1063/1.456294. URL <http://scitation.aip.org/content/aip/journal/jcp/90/11/10.1063/1.456294>.
44. B. Han, C. E. Carlton, J. Suntivich, Z. Xu, and Y. Shao-Horn. Oxygen reduction activity and stability trends of bimetallic pt0.5m0.5 nanoparticle in acid. *The*

Journal of Physical Chemistry C, 0(0):null, 0. doi: 10.1021/jp5129904. URL <http://dx.doi.org/10.1021/jp5129904>.

45. B. Hendriksen and J. Frenken. Co oxidation on pt(110): Scanning tunneling microscopy inside a high-pressure flow reactor. 89:0461011, 2002.
46. K. Honkala, P. Pirilä, and K. Laasonen. CO and NO adsorption and co-adsorption on the Pd(111) surface. *Surf. Sci.*, 489(1–3):72 – 82, 2001. ISSN 0039-6028. doi: [http://dx.doi.org/10.1016/S0039-6028\(01\)01135-9](http://dx.doi.org/10.1016/S0039-6028(01)01135-9). URL <http://www.sciencedirect.com/science/article/pii/S0039602801011359>.
47. H. Hopster and H. Ibach. Adsorption of co on pt(111) and pt 6(111) x (111) studied by high resolution electron energy loss spectroscopy and thermal desorption spectroscopy. *Surface Science*, 77:109, April 1978.
48. R. Huang, Y.-H. Wen, Z.-Z. Zhu, and S.-G. Sun. Pt–pd bimetallic catalysts: Structural and thermal stabilities of core–shell and alloyed nanoparticles. *J. Phys. Chem. C*, 116(15):8664–8671, 2012. doi: 10.1021/jp3015639. URL <http://dx.doi.org/10.1021/jp3015639>.
49. S. Izvekov, M. R. Philpott, and R. I. Eglitis. Ab initio simulation of metal cluster surrounded by electrolyte. *J. Electrochem. Soc.*, 147(6):2273–2278, Jun 2000. ISSN 0013-4651. doi: 10.1149/1.1393520.
50. H. Jeong and E. Williams. Steps on surfaces: experiment and theory. *SURFACE SCIENCE REPORTS*, 34(6-8):171–294, 1999. ISSN 0167-5729. doi: {10.1016/S0167-5729(98)00010-7}.
51. H.-C. Jeong and E. D. Williams. Steps on surfaces: experiment and theory. *Surface Science Reports*, 34(6–8):171 – 294, 1999. ISSN 0167-5729. doi: [http://dx.doi.org/10.1016/S0167-5729\(98\)00010-7](http://dx.doi.org/10.1016/S0167-5729(98)00010-7). URL <http://www.sciencedirect.com/science/article/pii/S0167572998000107>.
52. R. A. Johnson. Alloy models with the embedded-atom method. 39(17):12554, 1989.
53. S. Kelemen, T. Fischer, and J. Schwarz. The binding energy of CO on clean and sulfur covered platinum surfaces. *Surf. Sci.*, pages 440–450, 1979.
54. H. Y. Kim and G. Henkelman. CO adsorption-driven surface segregation of Pd on Au/Pd bimetallic surfaces: Role of defects and effect on co oxidation. *ACS Catalysis*, 3(11):2541–2546, 2013. doi: 10.1021/cs4006259. URL <http://dx.doi.org/10.1021/cs4006259>.
55. H. Y. Kim and G. Henkelman. CO adsorption-driven surface segregation of pd on Au/Pd bimetallic surfaces: Role of defects and effect on CO oxidation. *ACS Catalysis*, 3(11):2541–2546, 2013. doi: 10.1021/cs4006259. URL <http://dx.doi.org/10.1021/cs4006259>.

56. Y. Kimura, T. Cagin, and W. Goddard III. The quantum sutton-chen many body potential for properties of fcc metals, 1998. URL <http://csdrm.caltech.edu/publications/cit-asci-tr/cit-asci-tr003.pdf>.
57. C. Korzeniewski, S. Pons, P. P. Schmidt, and M. W. Severson. A theoretical analysis of the vibrational spectrum of carbon monoxide on platinum metal electrodes. *J. Chem. Phys.*, 85:4153, June 1986.
58. G. Kresse and J. Hafner. Ab initio molecular-dynamics for open-shell transition-metals. 48(17):13115–13118, Nov 1993. ISSN 0163-1829. doi: 10.1103/PhysRevB.48.13115.
59. G. Kresse and J. Hafner. Ab initio molecular-dynamics for liquid-metals. 47(1): 558–561, Jan 1993. ISSN 0163-1829. doi: 10.1103/PhysRevB.47.558.
60. G. Kresse and J. Hafner. Ab-initio molecular-dynamics simulation of the liquid-metal amorphous-semiconductor transition in germanium. 49(20):14251–14269, May 1994. ISSN 0163-1829. doi: 10.1103/PhysRevB.49.14251.
61. G. Kresse and D. Joubert. From ultrasoft pseudopotentials to the projector augmented-wave method. 59(3):1758–1775, Jan 1999. doi: 10.1103/PhysRevB.59.1758.
62. J. Kugai, J. T. Miller, N. Guo, and C. Song. Oxygen-enhanced water gas shift on ceria-supported pd–cu and pt–cu bimetallic catalysts. *J. Catal.*, 277 (1):46 – 53, 2011. ISSN 0021-9517. doi: <http://dx.doi.org/10.1016/j.jcat.2010.10.014>. URL <http://www.sciencedirect.com/science/article/pii/S0021951710003714>.
63. J. Larsen and I. Chorkendorff. From fundamental studies of reactivity on single crystals to the design of catalysts. *SURFACE SCIENCE REPORTS*, 35(5-8): 165–222, 1999. ISSN 0167-5729.
64. B. Lim, M. Jiang, P. H. C. Camargo, E. C. Cho, J. Tao, X. Lu, Y. Zhu, and Y. Xia. Pd-pt bimetallic nanodendrites with high activity for oxygen reduction. *Science*, 324(5932):1302–1305, 2009. doi: 10.1126/science.1170377. URL <http://www.sciencemag.org/content/324/5932/1302.abstract>.
65. S. Limpattayanate and M. Hunsom. Electrocatalytic activity of pt–pd electrocatalysts for the oxygen reduction reaction in proton exchange membrane fuel cells: Effect of supports. *Renewable Energy*, 63(0):205 – 211, 2014. ISSN 0960-1481. doi: <http://dx.doi.org/10.1016/j.renene.2013.09.014>. URL <http://www.sciencedirect.com/science/article/pii/S0960148113004813>.
66. L. Liu, G. Samjeske, S.-i. Nagamatsu, O. Sekizawa, K. Nagasawa, S. Takao, Y. Imaizumi, T. Yamamoto, T. Uruga, and Y. Iwasawa. Enhanced oxygen reduction reaction activity and characterization of pt–pd/c bimetallic fuel cell catalysts with pt-enriched surfaces in acid media. *J. Phys. Chem. C*, 116(44):

- 23453–23464, 2012. doi: 10.1021/jp308021a. URL <http://dx.doi.org/10.1021/jp308021a>.
67. D. Loffreda, D. Simon, and P. Sautet. Dependence of stretching frequency on surface coverage and adsorbate–adsorbate interactions: a density-functional theory approach of CO on Pd (111). *Surf. Sci.*, 425(1):68 – 80, 1999. ISSN 0039-6028. doi: [http://dx.doi.org/10.1016/S0039-6028\(99\)00186-7](http://dx.doi.org/10.1016/S0039-6028(99)00186-7). URL <http://www.sciencedirect.com/science/article/pii/S0039602899001867>.
 68. J. Lu and J. A. Szpunar. Applications of the embedded-atom method to glass formation and crystallization of liquid and glass transition-metal nickel. *Phil. Mag. A*, 75:1057–1066, 1997.
 69. Y.-C. Lu, H. A. Gasteiger, and Y. Shao-Horn. Catalytic activity trends of oxygen reduction reaction for nonaqueous li-air batteries. *J. Am. Chem. Soc.*, 133(47):19048–19051, 2011. doi: 10.1021/ja208608s. URL <http://dx.doi.org/10.1021/ja208608s>.
 70. S. E. Mason, I. Grinberg, and A. M. Rappe. First-principles extrapolation method for accurate co adsorption energies on metal surfaces. *Phys. Rev. B*, 69: 161401, April 2004.
 71. D. N. McCarthy, C. E. Strelbel, T. P. Johansson, a. den Dunnen, a. Nierhoff, J. H. Nielsen, and I. Chorkendorff. Structural modification of platinum model systems under high pressure CO annealing. *J. Phys. Chem. C*, 116(29):15353–15360, 2012. ISSN 1932-7447. doi: 10.1021/jp302379x. URL <http://pubs.acs.org/doi/abs/10.1021/jp302379x>.
 72. B. Medasani, Y. H. Park, and I. Vasiliev. Theoretical study of the surface energy, stress, and lattice contraction of silver nanoparticles. 75, 2007. doi: ARTN235436.
 73. M. A. Meineke, C. F. Vardeman, T. Lin, C. J. Fennell, and J. D. Gezelter. OOPSE: An object-oriented parallel simulation engine for molecular dynamics. *J. Comput. Chem.*, 26(3):252–271, 2005. ISSN 1096-987X. doi: 10.1002/jcc.20161. URL <http://dx.doi.org/10.1002/jcc.20161>.
 74. J. R. Michalka, P. W. McIntyre, and J. D. Gezelter. Molecular dynamics simulations of the surface reconstructions of Pt(557) and Au(557) under exposure to CO. *J. Phys. Chem. C*, 117(28):14579–14587, 2013. doi: 10.1021/jp402798n. URL <http://pubs.acs.org/doi/abs/10.1021/jp402798n>.
 75. Y. Mishin, D. Farkas, M. J. Mehl, and D. A. Papaconstantopoulos. Interatomic potentials for monoatomic metals from experimental data and ab initio calculations. 59(5):3393–3407, 1999. URL <http://link.aps.org/abstract/PRB/v59/p3393>.

76. Y. Mishin, M. J. Mehl, D. A. Papaconstantopoulos, A. F. Voter, and J. D. Kress. Structural stability and lattice defects in copper: *Ab initio*, tight-binding, and embed-ded-atom methods. 63:224106, June 2001. URL <http://link.aps.org/abstract/PRB/v63/e224106>.
77. Y. Mishin, M. J. Mehl, and D. A. Papaconstantopoulos. Embedded-atom potential for b2-nial. 65(22):224114, June 2002. URL <http://link.aps.org/abstract/PRB/v65/e224114>.
78. Y. Mishin, M. Mehl, and D. Papaconstantopoulos. Phase stability in the fe-ni system: Investigation by first-principles calculations and atomistic simulations. *Acta Mat.*, 53(15):4029–4041, September 2005. URL <http://dx.doi.org/10.1016/j.actamat.2005.05.001>.
79. H. J. Monkhorst and J. D. Pack. Special points for brillouin-zone integrations. *Phys. Rev. B*, 13:5188–5192, Jun 1976. doi: 10.1103/PhysRevB.13.5188. URL <http://link.aps.org/doi/10.1103/PhysRevB.13.5188>.
80. A. Morlang, U. Neuhausen, K. Klementiev, F.-W. Schütze, G. Miehe, H. Fuess, and E. Lox. Bimetallic pt/pd diesel oxidation catalysts: Structural characterisation and catalytic behaviour. *Appl. Catal., B*, 60(3–4):191 – 199, 2005. ISSN 0926-3373. doi: <http://dx.doi.org/10.1016/j.apcatb.2005.03.007>. URL <http://www.sciencedirect.com/science/article/pii/S0926337305001657>.
81. H. Ohtani, M. A. V. Hove, and G. A. Somorjai. LEED intensity analysis of the surface structures of Pd(111) and of CO adsorbed on Pd(111) in a $(\sqrt{3} \times \sqrt{3})r30^\circ$ arrangement. *Surf. Sci.*, 187(2–3):372–386, 9 1987. doi: [http://dx.doi.org/10.1016/S0039-6028\(87\)80063-8](http://dx.doi.org/10.1016/S0039-6028(87)80063-8). URL <http://www.sciencedirect.com/science/article/pii/S0039602887800638>.
82. J. D. Padmos, M. Langman, K. MacDonald, P. Comeau, Z. Yang, M. Filaggi, and P. Zhang. Correlating the atomic structure of bimetallic silver–gold nanoparticles to their antibacterial and cytotoxic activities. *The Journal of Physical Chemistry C*, 0(0):null, 0. doi: 10.1021/acs.jpcc.5b00145. URL <http://dx.doi.org/10.1021/acs.jpcc.5b00145>.
83. T. P. Pearl and S. J. Sibener. Oxygen driven reconstruction dynamics of ni(977) measured by time-lapse scanning tunneling microscopy. *J. Chem. Phys.*, 115(4): 1916, July 2001.
84. J. P. Perdew, K. Burke, and M. Ernzerhof. Generalized gradient approximation made simple. *Phys. Rev. Lett.*, 77:3865–3868, Oct 1996. doi: 10.1103/PhysRevLett.77.3865. URL <http://link.aps.org/doi/10.1103/PhysRevLett.77.3865>.
85. K. Peters, P. Steadman, H. Isern, J. Alvarez, and S. Ferrer. Elevated-pressure chemical reactivity of carbon monoxide over au(111). *Surface Science*, 467: 10–22, August 2000.

86. L. Piccolo, D. Loffreda, F. J. C. S. Aires, C. Deranlot, Y. Jugnet, P. Sautet, and J. C. Bertolini. The adsorption of co on au(111) at elevated pressures studied by stm, rairs, and dft calculations. *Surface Science*, 566–568:995–1000, June 2004.
87. S. J. Plimpton and B. A. Hendrickson. Parallel molecular dynamics with the embedded atom method. *Mrs Proceedings*, 291:37, 1993.
88. Y. Qi, T. Cagin, Y. Kimura, and W. A. Goddard III. Molecular-dynamics simulations of glass formation and crystallization in binary liquid metals: Cu-Ag and Cu-Ni. 59(5):3527–3533, 1999.
89. A. M. Rappe, K. M. Rabe, E. Kaxiras, and J. D. Joannopoulos. Optimized pseudopotentials. *Phys. Rev. B*, 41:1227–1230, Jan 1990. doi: 10.1103/PhysRevB.41.1227. URL <http://link.aps.org/doi/10.1103/PhysRevB.41.1227>.
90. T. Reier, M. Oezaslan, and P. Strasser. Electrocatalytic oxygen evolution reaction (oer) on ru, ir, and pt catalysts: A comparative study of nanoparticles and bulk materials. *ACS Catalysis*, 2(8):1765–1772, 2012. doi: 10.1021/cs3003098. URL <http://dx.doi.org/10.1021/cs3003098>.
91. J. A. Rifkin, C. S. Becquart, D. Kim, and P. C. Clapp. *Dislocation Generation and Crack Propagation in Metals Examined in Molecular Dynamics Simulations*, volume 278 of *MRS Symp. Proc.*, page 173. 1992.
92. A. Rizzo, S. Coriani, A. Halkier, and C. Hättig. Ab initio study of the electric-field-gradient-induced birefringence of a polar molecule: Co. *J. Chem. Phys.*, 113:3077, May 2000.
93. A. Russell and W. S. Epling. Diesel oxidation catalysts. *Catalysis Reviews*, 53(4):337–423, 2011. doi: 10.1080/01614940.2011.596429. URL <http://dx.doi.org/10.1080/01614940.2011.596429>.
94. S. Sankaranarayanan, V. Bhethanabotla, and B. Joseph. Molecular dynamics simulation study of the melting of pd-pt nanoclusters. 71, 2005. doi: ARTN195415.
95. S. K. R. S. Sankaranarayanan, V. R. Bhethanabotla, and B. Joseph. Molecular dynamics simulation study of the melting of pd-pt nanoclusters. *Phys. Rev. B*, 71:195415, May 2005. doi: 10.1103/PhysRevB.71.195415. URL <http://link.aps.org/doi/10.1103/PhysRevB.71.195415>.
96. S. K. R. S. Sankaranarayanan, V. R. Bhethanabotla, and B. Joseph. Molecular dynamics simulations of the structural and dynamic properties of graphite-supported bimetallic transition metal clusters. *Phys. Rev. B*, 72:195405, Nov 2005. doi: 10.1103/PhysRevB.72.195405. URL <http://link.aps.org/doi/10.1103/PhysRevB.72.195405>.

97. S. K. R. S. Sankaranarayanan, V. R. Bhethanabotla, and B. Joseph. Molecular dynamics simulation study of the melting and structural evolution of bimetallic pd-pt nanowires. 74(15):155441, 2006. URL <http://link.aps.org/abstract/PRB/v74/e155441>.
98. E. Schweizer, B. Persson, M. Tüshaus, D. Hoge, and A. Bradshaw. The potential energy surface, vibrational phase relaxation and the order-disorder transition in the adsorption system pt111-co. *Surface Science*, 213(1):49 – 89, 1989. ISSN 0039-6028. doi: [http://dx.doi.org/10.1016/0039-6028\(89\)90252-5](http://dx.doi.org/10.1016/0039-6028(89)90252-5). URL <http://www.sciencedirect.com/science/article/pii/0039602889902525>.
99. M. Shao, G. He, A. Peles, J. H. Odell, J. Zeng, D. Su, J. Tao, T. Yu, Y. Zhu, and Y. Xia. Manipulating the oxygen reduction activity of platinum shells with shape-controlled palladium nanocrystal cores. *Chem. Comm.*, 49(79):9030–2, 2013. ISSN 1364-548X. doi: [10.1039/c3cc43276a](https://doi.org/10.1039/c3cc43276a). URL <http://www.ncbi.nlm.nih.gov/pubmed/23982335>.
100. V. Shastry and D. Farkas. Molecular statics simulation of fracture in alpha-iron. *Modelling and Simulation In Materials Science and Engineering*, 4:473–492, 1996.
101. V. Shastry and D. Farkas. Atomistic simulation of fracture in coal and feal. *Intermetallics*, 6:95–104, 1998.
102. T. Shibata, B. Bunker, Z. Zhang, D. Meisel, C. Vardeman II, and J. Gezelter. Size-dependent spontaneous alloying of au-ag nanoparticles. 124:11989–11996, 2002. doi: DOI10.1021/ja025764r.
103. J. L. D. Silva, C. Stampfl, and M. Scheffler. Converged properties of clean metal surfaces by all-electron first-principles calculations. *Surf. Sci.*, 600(3): 703 – 715, 2006. ISSN 0039-6028. doi: <http://dx.doi.org/10.1016/j.susc.2005.12.008>. URL <http://www.sciencedirect.com/science/article/pii/S0039602805013154>.
104. B. T. Snead, A. P. Young, D. Jalalpoor, M. C. Golden, S. Mao, Y. Jiang, Y. Wang, and C.-K. Tsung. Shaped pd–ni–pt core-sandwich-shell nanoparticles: Influence of ni sandwich layers on catalytic electrooxidations. *ACS Nano*, 8 (7):7239–7250, 2014. doi: [10.1021/nn502259g](https://doi.org/10.1021/nn502259g). URL <http://dx.doi.org/10.1021/nn502259g>.
105. V. R. Stamenkovic, B. Fowler, B. S. Mun, G. Wang, P. N. Ross, C. A. Lucas, and N. M. Marković. Improved oxygen reduction activity on Pt₃Ni(111) via increased surface site availability. *Science*, 315(5811):493–497, 2007. doi: [10.1126/science.1135941](https://doi.org/10.1126/science.1135941). URL <http://www.sciencemag.org/content/315/5811/493.abstract>.

106. J. E. Straub and M. Karplus. Molecular dynamics study of the photodissociation of carbon monoxide from myoglobin: Ligand dynamics in the first 10 ps. *Chem. Phys.*, 158:221–248, June 1991.
107. S. Surnev, M. Sock, M. Ramsey, F. Netzer, M. Wiklund, M. Borg, and J. Andersen. CO adsorption on pd(111): a high-resolution core level photoemission and electron energy loss spectroscopy study. *Surf. Sci.*, 470 (1–2):171 – 185, 2000. ISSN 0039-6028. doi: [http://dx.doi.org/10.1016/S0039-6028\(00\)00853-0](http://dx.doi.org/10.1016/S0039-6028(00)00853-0). URL <http://www.sciencedirect.com/science/article/pii/S0039602800008530>.
108. A. P. Sutton and J. Chen. Long-range finnis sinclair potentials. *Phil. Mag. Lett.*, 61:139–146, 1990.
109. J. Szanyi, W. K. Kuhn, and D. W. Goodman. CO adsorption on Pd(111) and Pd(100): Low and high pressure correlations. *J. Vac. Sci. Technol. A*, 11(4):1969–1974, 1992.
110. F. Tao and M. Salmeron. In situ studies of chemistry and structure of materials in reactive environments. *Science*, 331:171, Jan 2011.
111. F. Tao, M. E. Grass, Y. Zhang, D. R. Butcher, J. R. Renzas, Z. Liu, J. Y. Chung, B. S. Mun, M. Salmeron, and G. A. Somorjai. Reaction-driven restructuring of rh-pd and pt-pd core-shell nanoparticles. *Science*, 322:932, November 2008.
112. F. Tao, M. E. Grass, Y. Zhang, D. R. Butcher, J. R. Renzas, Z. Liu, J. Y. Chung, B. S. Mun, M. Salmeron, and G. A. Somorjai. Reaction-driven restructuring of rh-pd and pt-pd core-shell nanoparticles. *Science*, 322(5903):932–934, 2008. doi: 10.1126/science.1164170. URL <http://www.sciencemag.org/content/322/5903/932.abstract>.
113. F. Tao, S. Dag, L.-W. Wang, Z. Liu, D. R. Butcher, H. Bluhm, M. Salmeron, and G. A. Somorjai. Break-up of stepped platinum catalyst surfaces by high co coverage. *Science*, 327(5967):850–853, 2010.
114. F. Tao, S. Dag, L.-W. Wang, Z. Liu, D. R. Butcher, H. Bluhm, M. Salmeron, and G. A. Somorjai. Break-up of stepped platinum catalyst surfaces by high co coverage. *Science*, 327(5967):850–853, 2010. doi: 10.1126/science.1182122. URL <http://www.sciencemag.org/content/327/5967/850.abstract>.
115. P. Thostrup, E. Christoffersen, H. T. Lorensen, K. W. Jacobsen, F. Besenbacher, and J. K. Nørskov. Adsorption-induced step formation. *Phys. Rev. Lett.*, 87 (12):126102, 2001. ISSN 0031-9007. doi: 10.1103/PhysRevLett.87.126102.
116. X. Tuaev, S. Rudi, V. Petkov, A. Hoell, and P. Strasser. In situ study of atomic structure transformations of pt–ni nanoparticle catalysts during electrochemical potential cycling. *ACS Nano*, 7(7):5666–5674, 2013. doi: 10.1021/nn402406k. URL <http://dx.doi.org/10.1021/nn402406k>.

117. W. Tyson and W. Miller. Surface free energies of solid metals: Estimation from liquid surface tension measurements. *Surf. Sci.*, 62(1):267 – 276, 1977. ISSN 0039-6028. doi: [http://dx.doi.org/10.1016/0039-6028\(77\)90442-3](http://dx.doi.org/10.1016/0039-6028(77)90442-3). URL <http://www.sciencedirect.com/science/article/pii/0039602877904423>.
118. P. van Beurden, H. Verhoeven, G. Kramer, and B. Thijssse. Atomistic potential for adsorbate/surface systems: Co on pt. 66(23):235409, Dec. 2002. doi: DOI10.1103/PhysRevB.66.235409.
119. A. F. Voter. The embedded-atom method. *Intermetallic Compounds: Principles and Practice*, 1:77, 1995.
120. A. F. Voter. *The Embedded-Atom Method*, volume 1, Principles, chapter 4, pages 77–90. John Wiley & Sons Ltd., 1994.
121. G. Wang, M. Van Hove, P. Ross, and M. Baskes. Surface structures of cubo-octahedral pt-mo catalyst nanoparticles from monte carlo simulations. 109: 11683–11692, 2005. doi: DOI10.1021/jp050116n.
122. E. D. Williams. Surface steps and surface morphology: understanding macroscopic phenomena from atomic observations. *Surface Science*, 299/300:502–524, 1994.
123. E. D. Williams and N. C. Bartelt. Thermodynamics of surface morphology. *Science*, 251:393–400, January 1991.
124. Y. T. Wong and R. Hoffmann. Chemisorption of carbon monoxide on three metal surfaces: nickel(111), palladium(111), and platinum(111): a comparative study. *J. Phys. Chem.*, 95(2):859–867, 1991. doi: 10.1021/j100155a069. URL <http://dx.doi.org/10.1021/j100155a069>.
125. Y. Yang, Z. Zhao, R. Cui, H. Wu, and D. Cheng. Structures, thermal stability, and chemical activity of crown-jewel-structured pd-pt nanoalloys. *J. Phys. Chem. C*, 2015. doi: 10.1021/jp5107108. URL <http://dx.doi.org/10.1021/jp5107108>.
126. Y. Y. Yeo, L. Vattuone, and D. A. King. Calorimetric heats for co and oxygen adsorption and for the catalytic co oxidation reaction on pt111. *J. Chem. Phys.*, 106:392–402, January 1997.
127. Y. Y. Yeo, L. Vattuone, and D. A. King. Calorimetric heats for CO and oxygen adsorption and for the catalytic CO oxidation reaction on Pt(111). *J. Chem. Phys.*, 106:392–402, January 1997.
128. Y. Yu, O. Y. Gutiérrez, G. L. Haller, R. Colby, B. Kabius, J. R. van Veen, A. Jentys, and J. A. Lercher. Tailoring silica-alumina-supported pt-pd as poison-tolerant catalyst for aromatics hydrogenation. *J. Catal.*, 304(0):135 – 148, 2013. ISSN 0021-9517. doi: <http://dx.doi.org/10.1016/j.jcat.2013.04.009>. URL <http://www.sciencedirect.com/science/article/pii/S0021951713001322>.

129. J. Zhang, K. Sasaki, E. Sutter, and R. R. Adzic. Stabilization of platinum oxygen-reduction electrocatalysts using gold clusters. *Science*, 315(5809):220–222, 2007. doi: 10.1126/science.1134569. URL <http://www.sciencemag.org/content/315/5809/220.abstract>.
130. J. Zhang, K. Sasaki, E. Sutter, and R. R. Adzic. Stabilization of platinum oxygen-reduction electrocatalysts using gold clusters. *Science*, 315(5809):220–222, 01 2007. URL <http://www.sciencemag.org/content/315/5809/220.abstract>. N2-Wedemonstratedthatplatinum(Pt) oxygen-reductionfuel-cellelectrocatalystscanbestabilizedagainstdissolutionunderyby modifyingPtinanoparticleswithgold(Au)clusters. ThisbehaviorwasobservedundertheoxidizingconditionsoftheO₂reductionreactionandp6and1.1voltsinover30,000cycles. Therewereinsignificantchangesintheactivityandsu in contrasttosizablelossesobservedwiththepurePt catalystunderthesameconditions. Insitu x-rayabsorptionnear-edgespectroscopyandvoltammetrydatasuggestthattheAuCl
131. P. Zhang, Y. Hu, B. Li, Q. Zhang, C. Zhou, H. Yu, X. Zhang, L. Chen, B. Eichhorn, and S. Zhou. Kinetically stabilized pd@pt core–shell octahedral nanoparticles with thin pt layers for enhanced catalytic hydrogenation performance. *ACS Catalysis*, 5(2):1335–1343, 2015. doi: 10.1021/cs501612g. URL <http://dx.doi.org/10.1021/cs501612g>.
132. X. Zhang, S. Yu, L. Qiao, W. Zheng, and P. Liu. Stabilization of pt monolayer catalysts under harsh conditions of fuel cells. *The Journal of Chemical Physics*, 142(19):194710, 2015. doi: <http://dx.doi.org/10.1063/1.4921257>. URL <http://scitation.aip.org/content/aip/journal/jcp/142/19/10.1063/1.4921257>.
133. R. R. Zope and Y. Mishin. Interatomic potentials for atomistic simulations of the ti-al system. 68:024102, July 2003. URL <http://link.aps.org/abstract/PRB/v68/e024102>.

This document was prepared & typeset with pdfL^AT_EX, and formatted with NDDiss2_ε classfile (v3.2013[2013/04/16]) provided by Sameer Vijay and updated by Megan Patnott.